Three major types of subcontinental lithospheric mantle beneath the Variscan orogen in Europe

Jacek Puziewicz, Magdalena Matusiak-Malek, Theodoros Ntaflos, Michel Grégoire, Mary-Alix Kaczmarek, Sonja Aulbach, Malgorzata Ziobro, Anna Kukula

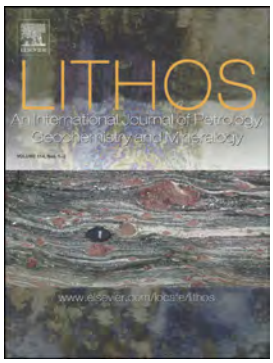

Three major types of subcontinental lithospheric mantle beneath the Variscan orogen in Europe

Jacek Puziewicz, Magdalena Matusiak-Małek, Theodoros Ntaflos, Michel Grégoire, Mary-Alix Kaczmarek, Sonja Aulbach, Małgorzata Ziobro, Anna Kukuła

PII: S0024-4937(20)30104-3

DOI: https://doi.org/10.1016/j.lithos.2020.105467

Reference: LITHOS 105467

To appear in: *LITHOS*

Received date: 24 June 2019

Revised date: 29 February 2020

Accepted date: 3 March 2020

Please cite this article as: J. Puziewicz, M. Matusiak-Małek, T. Ntaflos, et al., Three major types of subcontinental lithospheric mantle beneath the Variscan orogen in Europe, *LITHOS*(2020), https://doi.org/10.1016/j.lithos.2020.105467

Three major types of subcontinental lithospheric mantle beneath the Variscan orogen in Europe

Jacek Puziewicz[1], Magdalena Matusiak-Małek[1], Theodoros Ntaflos[2], Michel Grégoire[3], Mary-Alix Kaczmarek[3], Sonja Aulbach[4], Małgorzata Ziobro[1], Anna Kukuła[5]

[1] Institute of Geological Sciences, University of Wrocław, Wrocław, Poland
[2] Department of Lithospheric Research, University of Vienna, Vienna, Austria
[3] Géosciences Environnement Toulouse (GET), Observatoire Midi- Pyrénées, CNRS-CNES-IRD-Université Toulouse III, Toulouse, France
[4] Institut für Geowissenschaften, Goethe Universität, Frankfurt am Main, Germany
[5] Institute of Geological Sciences, Polish Academy of Sciences, Warsaw, Poland

Abstract. Petrographic observations as well as new and published mineral major and trace element compositions, in part complemented by electron backscatter diffraction, evidence that representative mantle xenolith suites from several Cenozoic basalt locations in the European Variscan orogen can be grouped into three main types. Each type is derived from parts of the sub-continental lithospheric mantle which have experienced a different geological history. The oldest type, referred to as orogenic mantle, is dominated by strongly depleted harzburgites, which represent a fossil Variscan mantle wedge with slices of mantle of continental and oceanic plates attached to it during collision. This mantle lithosphere has been overprinted by Cenozoic carbonated alkali basalt melts, and clinopyroxene, if present, is LREE-enriched and re-introduced. This type of mantle is exemplified by xenoliths from Lower Silesia (Poland) and the northern Massif Central (France). The second type of lithospheric mantle lies beneath parts of the Variscan orogen which experienced Cenozoic rifting. This mantle is dominated by harzburgites and lherzolites formed by multiple episodes of reactive percolation of basaltic melts generated at various stages of continental rifting. The clinopyroxene REE patterns range from flat to LREE-enriched. The xenoliths from Vogelsberg (Germany) are an example of such a lithospheric mantle. The third mantle type consists of lherzolites which originated by refertilization of a harzburgitic protolith by melts derived from upwelled asthenosphere. Lherzolites contain primary clinopyroxene characterized by LREE-depleted-patterns. The xenoliths from south Massif Central (France) are an example of that third type.

The xenoliths in Cenozoic basalts considered so far show that the mantle root of the Variscan orogen in Central Europe consists of various domains which in part conserve their characteristics from the time of the Variscan collision, and in part are

overprinted by metasomatism caused by late-orogenic asthenosphere upwelling or by Cenozoic rifting. The metasomatically affected domains are decoupled from the Variscan structure of the orogen.

Keywords: lithospheric mantle, variation, metasomatism, Variscan orogen, Europe

1. Introduction

The European Variscan orogen originated in Upper Palaeozoic times (e. g. Kroner and Romer 2013), and was reactivated in the Cenozoic, when a system of rifts was formed due to stresses related to the Alpine orogeny (Dèzes et al. 2004). Rifting was connected with alkaline, mostly basaltic volcanism, which was active in the rifts and neighbouring Variscan basement elevations (Wilson and Downes 1990). In many places, alkali basalt lavas entrained mantle xenoliths, which allows the lithospheric mantle root of the orogen to be studied. Numerous xenolith occurrences and active quarrying, giving access to unweathered xenoliths, offer the opportunity to compare the nature of the mantle roots underlying various parts of the orogen.

The study of Downes (2001) showed that the lithospheric mantle beneath Europe consists of spinel lherzolites grading to spinel harzburgites, which have been subjected to significant melting and subsequently modified by various metasomatic processes and events. In consequence, the European subcontinental lithospheric mantle (SCLM) shows lithological variation. Two lithologically different SCLM domains beneath the Massif Central in France were recognized in the xenolith studies of Lenoir et al. (2000) and Downes et al. (2003). Puziewicz et al. (2015) showed that the SCLM domain beneath Lower Silesia in Poland is dominated by harzburgites, which contain orthopyroxene that is significantly more Al-poor than those occurring to the west. Thus, the Lower Silesian domain differs from those located to the west. However, a systematic study of SCLM variation at the European scale is missing.

In this paper we present xenolith-based petrological data documenting peridotite variation in the SCLM underlying the Variscan orogen in Central Europe from Lower

Silesia in the east to French Massif Central in the west (Fig. 1). To define the differences among various lithospheric mantle lithologies, we use the mineral chemical data collected by us with the identical set of analytical methods (electron microprobe and LA-ICP-MS) supplemented, when necessary, by electron backscatter diffraction (EBSD) study to obtain more detailed information about the microstructure. We use our older published data from Lower Silesia in Poland (Puziewicz 2015 and references therein) and present some new "representative examples" from Vogelsberg (Germany) and Massif Central (France). We show that large parts of the Variscan lithospheric mantle were metasomatically rejuvenated in the post-Variscan times and/or during Cenozoic rifting, but the slices of sub-oceanic mantle accreted to the growing Variscan orogen can be recognised in places.

2. Geological background and rationale

The "standard" Phanerozoic orogen originates by accretion of a continental plate to a continental margin during subduction and eventual closure of an ocean (e. g. Kearey et al., 2008). The mantle of the overriding plate forms a "mantle wedge", subjected to reactive migration of melts and fluids released from the subducted plate. The evolution of the Variscan orogen of Europe fits this model: it was formed in Devonian-Carboniferous by assembly of relatively small, Gondwana-derived "microcontinental" plates (Franke 2014 and references therein). The orogen consists of major accretionary terranes, which are readily recognizable in the upper- and middle crust. The boundaries between these terranes are, however, not visible in seismic studies of the lower crust (Meier et al. 2016 and references therein). The Moho beneath the orogen is flat and typically between 28-32 km (e.g. Meier et al. 2016). The study of Henk (1999) shows that the thickness of crust formed during the

collision was reduced by extensional stresses and gravitational collapse, and that extension was concentrated in lower crust. In this model, the mantle root of the Variscan orogen, formed during collision, was not removed by delamination. This is shown by differences in seismic anisotropy between parts of the SCLM underlying the major terranes of the Variscan orogen (Babuška and Plomerová 2006, Plomerová and Babuška, 2010). Nevertheless, parts of the Variscan SCLM must have locally delaminated in the late-orogenic stage and were replaced by upwelled asthenosphere, the melting of which triggered Stephanian-Early Permian volcanism in Central Europe (e. g. Ziegler and Dèzes 2005).

During the Cretaceous and Cenozoic, the Variscan orogen was subjected to intense rifting and volcanism affecting the foreland of the Alpine orogen (Dèzes et al. 2004). The concomitant thermal erosion of the lithosphere-asthenosphere boundary possibly caused significant asthenosphere upwellings in places (e. g. Meier et al. 2016). Rifting was connected with intense basaltic, mostly alkaline, volcanism, which formed the Central European Volcanic Province (CEVP), first defined by Wimmenauer (1974). The lavas of this province often carry lithospheric mantle xenoliths. The xenolith suites in individual sites come from the lithospheric mantle column located between the Moho (ca. 30 km) and the base of the lithosphere (currently typically 90-100 km), shallowing to ca. 60 km beneath the Upper Rhine Rift and to ca. 40 km beneath the Eifel Mts. (Babuška et al. 2010; Plomerová and Babuška, 2010; Seiberlich et al. 2013). Xenoliths can be entrained from various levels of the SCLM column, and the question of their representativeness is the major one behind xenolith-based petrological studies of SCLM. However, if relatively large xenolith populations are studied, and the results are reproducible regionally, it can be

assumed that the common xenolith types represent major SCLM lithologies beneath the region. This approach forms the foundation of this study.

The xenoliths brought to the surface by mafic magmas are commonly subjected to reactive melt infiltration preceding eruption. It is recorded as “fine-grained aggregates”, sometimes glass-bearing, which occur commonly in mantle peridotite xenoliths (e. g. Lu et al. 2015; Matusiak-Małek et al. 2013; Bali et al. 2002, Shaw and Klügel 2002). Minerals occurring in these aggregates (typically olivine and clinopyroxene ± opaques) have compositions typical of mantle, indicating that melt infiltrated and reacted with peridotite host at mantle depths (op. cit.). Fine-grained texture and glass occurrence show that they are the snap-shot of melt percolation occurring at the time of, or immediately preceding, xenolith entrainment. The time scale of those percolation events supposedly corresponds to the time-span of activity of related volcanic systems, which are up to ca. 3 million years (e. g. Vogelsberg volcano, Bogaard and Wörner 2003).

The effects of reactive melt infiltration which precedes xenolith entrainment and host lava eruption are easy to recognize because of their textural appearance, described above. However, the xenolith-based studies usually show that lithospheric mantle evolves through a sequence of multiple melt depletion and metasomatic events. The mantle peridotite xenolith suites can be grouped in two classes with this respect:

(1) suites consisting of xenoliths which record two or more major events (peridotites consisting of minerals formed by event 1, peridotites consisting of minerals formed by event 2, etc.);

(2) suites consisting of xenoliths which record also the transitional stages of rock transformation (peridotites consisting of minerals formed by event 1, peridotites

consisting of minerals formed by event 2, etc., and peridotites transitional between them).

In this study we describe xenolith suites which belong to the class (1) (Dreihausen in the Vogelsberg, Allègre and Alleyras in the Massif Central). They serve as "representative examples" which have been chosen from larger data set comprising also Heldburg Dike Swarm, Hessian Depression and Rhön Mts. (our unpublished data and conference abstracts: Ćwiek et al. 2018, Kukuła et al. 2017, 2018, Puziewicz et al. 2018). The example of a xenolith suite belonging to class (2) described in this study is that from Nidda in the Vogelsberg.

2.1. Regional geological context

In this paper we discuss xenolith suites from Lower Silesia (Poland), Vogelsberg (Germany) and the southern Massif Central (France). Those from Lower Silesia occur in lavas which erupted mostly in off-rift settings. The Vogelsberg volcano is located at the northern termination of the Upper Rhine Rift. The Massif Central xenolith suites described in this study come from the Devès volcanic field, situated in an off-rift setting.

2.1.1. Lower Silesia (SW Poland)

The north-eastern terminations of both the Variscan orogen and the CEVP lie in Lower Silesia (Fig. 1). Variscan basement comprises here (from west to east): the eastern part of the Saxo-Thuringian Zone, the Central Sudetes and the northern end of the Moravo-Silesian Zone (Fig. 2), which form the NE part of the Bohemian Massif. The Central Sudetes are considered to be the accretionary wedge formed during

Variscan subduction of the Saxo-Thuringia passive margin beneath the Brunia microcontinent (Mazur et al. 2015).

The Cenozoic alkaline basaltic volcanism in the Bohemian Massif is concentrated in the Eger (Ohře) Rift (Ulrych et al. 2011; Fig. 1). Smaller concentrations of Cenozoic lavas are located along the Odra-Labe fault system in Lower Silesia (Fig. 2), which is approximately perpendicular to the axis of the Eger Rift (Puziewicz et al. 2015 and references therein). Volcanic activity occurred at 30-26 and 22-18 Ma, with subordinate pulse at 5.5-3.8 Ma (Pécskay and Birkenmajer 2013). Almost all of the lavas are of basanite, nephelinite and (alkali) basalt (Ladenberger et al. 2006).

2.1.2. Vogelsberg (central Germany)

The Miocene lavas of Vogelsberg formed a shield volcano which was ca. 50 km in diameter (Ehrenberg and Hickenthier 1985). Vogelsberg is located at the northern tip of the Upper Rhine Graben (Fig. 3). The lavas overlie the contact between the Variscan Rheno-Hercynian Zone, the Northern Phyllite Zone and Mid-German Crystalline High (Fig. 3). Two latter units form the NW edge of the Saxo-Thuringian Zone the European Variscan orogen.

Lava ages vary between 18 and 14.7 Ma and the lava sequence starts with high-Ti basanites and their derivatives, overlain by alkali basalts and tholeiites and topped by basanites and primitive alkali basalts (Bogaard and Wörner 2003). The lavas come from both lithospheric and asthenospheric sources (Bogaard and Wörner 2003). Most of the mantle xenoliths occur in the asthenosphere-derived uppermost basanites and primitive alkali basalts (Bogaard and Wörner 2003). Witt-Eickschen (1993) revealed that xenoliths come from the mantle subjected to moderate melting followed by metasomatism.

2.1.3. Massif Central (France)

The French Massif Central comprises the largest occurrence of Cenozoic alkaline volcanic rocks in Europe, which are known for abundant mantle xenoliths. The volcanism occurred in three phases: (1) scattered eruptions at 65-38 Ma, (2) volcanism related to formation of the Limagne Graben at 38-15 Ma, and (3) later magmatic activity with peaks at 10-5 and 3.5-0.5 Ma (Michon and Merle 2001). The Devès volcanic field was formed during the youngest event (Michon and Merle 2001). The lavas from Massif Central comprise alkali basalts, basanites and their derivatives (Downes 1987).

The xenolith study of Lenoir et al. (2000) revealed two mantle domains beneath the region, one to the north of 45º30' N latitude which is more refractory and a more fertile one to the south. Lenoir et al. (2000) proposed that these two domains were assembled during the Variscan orogeny. Downes et al. (2003) showed that clinopyroxene Sr-Nd isotopic compositions in northern domain correspond to the European Asthenospheric Reservoir, whereas clinopyroxenes of the southern domain are MORB-like. Denyer-Thiele et al. (2017) corroborated the division and showed that this boundary is shifted slightly to the south (45º20' N).

3. Samples, methods and nomenclature

3.1 Samples

This study is based on new analytical data and on previously published work. The new data comprise xenoliths from Dreihausen quarry (Vogelsberg) and two xenolith suites from Massif Central: from the Ringue quarry near Allègre and from the vicinity of Alleyras (very old small quarry located to the south of village, noted by Coisy

1977). All the studied samples were fresh and unweathered. The samples for detailed study were chosen from larger set of xenoliths in order to represent the whole spectrum visible in thick sections and to avoid rocks exhibiting extensive melt infiltration. We examined thick sections from 46 xenoliths from Dreihausen to choose 14, 28 thick sections from Allègre to choose 8, and 13 thick sections from Alleyras to choose 6 for detailed study (Tables 1 and 2).

Each sample has been characterised by electron microprobe analyses of all phases and LA-ICP-MS analyses of clino- and orthopyroxene. Crystal preferred orientation in some samples from Massif Central has been studied by EBSD in order to verify the hypothesis based on mineral chemical data. The new data comprise also Nidda xenolith suite in Vogelsberg (18 samples, all collected xenoliths were studied), for comparison with the Dreihausen samples.

The previously published data comprise those on xenoliths from Lower Silesia and from Massif Central. The published data from Lower Silesia are by Ćwiek et al. (2016, 2018), Kukuła et al. (2015), Matusiak-Małek et al. (2010, 2014, 2017a, b) and Puziewicz et al. (2011, 2015). Data from Massif Central are from studies of Downes et al. (2003), Lenoir et al. (2000), Uenver-Thiele et al. (2014, 2017) and Zangana et al. (1997).

3.2. Methods

Modal compositions were determined on high-resolution images of thick sections by point-counting using JMicrovision software. Optical images and/or phase maps obtained with EBSD method, if available, were used. We used thick (100 μm) sections for both electron microprobe and LA-ICP-MS study.

Major element composition of minerals from Vogelsberg was analysed by Cameca SXFive FE electron microprobe at the Department of Lithospheric Research, University of Vienna, Austria. The minerals from Massif Central were analysed by Cameca SX 100 electron microprobe in the Microcharacterization Centre Raimond Castaing, University Paul Sabatier, Toulouse, France. Standard conditions were applied (acceleration voltage 15 kV, sample current 20/25 nA, counting times on peak position 20 s, background 10 s). To improve detection limits and accuracy, the counting time for Ca and Ni in olivine was slightly lengthened (peak 60 s, background 30 s). This allowed the detection limit of Ca in olivine to be ca. 160 ppm (0.02 wt. % CaO) and that of Ni in olivine and pyroxenes to be ca. 400 and 500 ppm (0.05 and 0.06 wt. % NiO). Mineral chemical data are summarized in Tables 1 and 2, the source data are given in Supplementary material 1a (Dreihausen in Vogelsberg) and Supplementary material 2a (Allègre and Alleyras in Massif Central).

Trace element contents in clinopyroxene and orthopyroxene were analysed by Laser Ablation ICP-MS technique. Sample runs were bracketed by measurements of NIST 612 glass which was used for sensitivity calibration (reference values of Jochum et al., 2011, were adopted). The Ca or Si content determined by electron microprobe was used as an internal standard for clinopyroxene, whereas Mg or Si contents were used for orthopyroxene. The spot diameter was 50 or 70 µm (clinopyroxene) and 70 to 100 µm (orthopyroxene). Samples from Vogelsberg were analysed at the Institut für Geowissenschaften, Goethe Universität (Frankfurt, Germany) using a RESOlution (Resonetics) 193 nm ArF Excimer Laser (CompexPro 102, Coherent), operated at a laser energy of 5 J/cm^2 and repetition rate of 8 Hz, coupled to a Thermo Scientific Element XR ICP-MS. Basalt glass BIR1G was used to monitor accuracy and in-house San Carlos orthopyroxene grain was used as

secondary standards (Aulbach et al. 2017). Results are reported in Supplementary material 3. Samples from the Massif Central were analysed in the laboratory of Géosciences Environnement Toulouse (CNRS-CNES-IRD-University Toulouse III), Observatoire Midi Pyrénées (Toulouse, France) using NewWave Research NWR213 Nd YAG 213 nm laser (laser energy 10.97 J/cm^2, repetition rate 10 Hz) and Thermo Scientific Element XR ICP-MS. NIST610 was used as secondary standard. The Glitter 4.0 software (van Achterberg *et al.,* 2001) was used for raw data processing. We analysed at least 2-4 grains of ortho- and clinopyroxene in each thick section. If the grain size allowed, 2 or 3 points in each grain were analysed (margin, centre and one point between). The grains proved to be homogeneous, as indicated by mostly low standard deviations of multiple spots, and the individual analyses were averaged (see Supplementary materials 1b and 2b, in which relative standard deviation is included). Relative standard deviation (rsd) is standard deviation of multiple analyses of each element in a sample, shown as a percent of average element concentration in the sample. This indicates whether there is homogeneity both at the grain and the sample scale and allows outliers to be identified.

For the Electron Backscatter Diffraction (EBSD) a mechanic-chemical polishing using a Vibromet was applied on thin sections for 1h15 with a colloidal silica suspension (pH 10) to remove mechanically-induced surface damage. EBSD data acquisition was performed with a JEOL 7100 microscope at the microcharacterization centre Raimond Castaing, University Paul Sabatier, Toulouse, France, equipped with an EBSD camera HKL Advanced Nordlys Nano from Oxford Instruments. The microscope working conditions include an acceleration voltage of 20 kV, a probe current of 16 nA, with a stage tilt of 70° and a working distance between 15 and 16

mm. Automatic indexing was performed using AZTec software (version 3.5) from Oxford Instruments, with different settings according to the grain size.

Data were processed using Channel 5 package. Measurements with a mean angular deviation (MAD) greater than 1.3 were removed, and grains were then calculated by imposing an orientation difference smaller than 10° for any two neighbouring measurements belong to the same grain. Grains with a surface smaller than 10 pixels were removed to avoid bias caused by potential indexing error. The maps were compared with band contrast maps to ensure that the treatment did not compromise the data. A lineation has been defined in the xenoliths, using clinopyroxene and orthopyroxene [001] axes, which are parallel and olivine [010] axes perpendicular to clinopyroxene and orthopyroxene [001] axes defining the pole to the foliation plane. For an easy comparison between the xenoliths, the poles figures have been oriented with the lineation sub-parallel to X within the defined foliation plane XY. The multiple uniform density (mud) and the J-index, which is the measure of fabric strength (Bunge, 1982) are reported on Fig. 16.

3.3. Nomenclature

Forsterite (Fo) content in olivine is calculated as atomic 100*Mg/(Mg+Fe+Mn) per formula unit. Spinel compositions were recalculated based on three cations, with Fe^{3+} and Fe^{2+} calculated by charge balance (Deer *et al*., 1993). The Cr-number (Cr#) stands for the atomic ratio of Cr/(Cr+Al), and Mg-number (Mg#) denotes atomic $Mg/(Mg+Fe^{tot.})$. Trace element contents were normalized to primitive mantle (PM) using McDonough and Sun (1995) values. We follow the textural terminology of Mercier and Nicolas (1975) in rock descriptions. In this paper we describe the primary minerals forming the xenoliths as “I” (olivine I, orthopyroxene I, etc., see also

Matusiak-Małek et al. 2014). Lamellae in primary minerals are referred to as “II” and minerals in fine-grained aggregates and forming reactive rims on primary ones are “III”.

4. Results

4.1. Vogelsberg xenolith suites

We present the results for the xenolith suite from Dreihausen quarry in the northern Vogelsberg (Fig. 3). The xenoliths are rounded, isometric to flattened, typically 5-12 cm in diameter. Their modal composition varies from harzburgite to clinopyroxene-poor lherzolite (Fig. 4). Olivine orthopyroxenite, clinopyroxenite and glimmerite xenoliths were also found. We additionally use the data on xenoliths from the Nidda quarry in the central part of Vogelsberg (Fig. 3, 18 samples). The mineral chemical data for Nidda are summarized in Supplementary material 4.

The Dreihausen xenolith suite shows two textural groups of xenoliths. The first comprises a single protogranular harzburgite (sample 3816). The second group consists of abundant, orthopyroxene-rich xenoliths with textures varying from slightly deformed protogranular (Fig. 5a, lherzolite 3824) through porphyroclastic (Fig. 5b, lherzolite 3841), to well-foliated (Fig. 5c, lherzolite 3843). We decided to classify harzburgite 3816 as a separate “group” because an analogous rock, in terms of texture and mineral chemistry, also occurs in the Nidda xenolith suite (see below).

The variable appearance of deformational structures in the deformed xenoliths of group 2 (Fig. 5b and d, lherzolites 3841 and 3828) is at least partly due to random sectioning, since in many instances we did not recognize foliation/lineation in hand-specimens. Spongy rims surround clinopyroxene in almost all xenoliths, and orthopyroxene in some. Spinel grains are commonly arranged in streaks following the

foliation of the silicate minerals. In porphyroclastic xenoliths, spinels are usually grouped in those parts of the rock affected by grain-size reduction (Fig. 5).

The undeformed harzburgite 3816 consists of olivine (Fo 91.3, NiO 0.40 wt. %; Fig. 6), Al-poor orthopyroxene (Mg# 0.92, 0.10 atoms of Al pfu; Fig. 7) and chromian spinel (Cr# 0.57, Fig. 6).

The deformed peridotites of group 2 (all samples in Fig. 6 except 3816) contain olivine with Fo 89.5 to 91.0. The pyroxenes (Mg# corresponds to that of olivine) are relatively aluminous: orthopyroxene contains 0.15 – 0.25 atoms of Al pfu (Fig. 7), whereas clinopyroxene has 0.20 – 0.33 atoms of Al pfu (Fig. 7). Spinel is aluminous (Cr# 0.10-0.25; Fig. 6). Harzburgite 3811 and lherzolite 3828 contain pyroxenes and spinel transitional between the Al-depleted undeformed harzburgite 3816 and Al-rich deformed peridotites (Figs. 7 and 8). The exception is harzburgite 3831, which contains orthopyroxene extremely depleted in Al (0.07 atoms of Al pfu) and spinel Cr# 0.61, is porphyroclastic, and contains olivine Fo 90.5 (Figs. 6, 7 and 8).

The REE/trace element patterns of pyroxenes are decoupled from major element characteristics so that the grouping of samples based on major element mineral compositions is different from that based on mineral REE/trace element content. The exception is harzburgite 3816 and its analogue from Nidda (harzburgite 3896), in which mineral major and REE/trace element define a single group comprising only two rocks. Orthopyroxene from harzburgite 3816 (pattern of Type I) has a sinusoidal REE pattern showing HREE-depletion and LREE-enrichment relative to orthopyroxenes from the deformed samples (Fig. 8). Orthopyroxene from the deformed peridotites shows 3 types of patterns (II, III and IV) differing by the degree of LREE depletion relative to HREE and shape (Fig. 8). The REE (Fig. 8) and trace

element (Fig. 9) patterns of clinopyroxene can also be grouped in types, which correspond to those defined by orthopyroxene.

The Nidda xenolith suite consists mainly of porphyroclastic or strongly foliated harzburgites and lherzolites. Protogranular texture is rare (only two harzburgites out of 18 samples). Two clinopyroxenite and one dunite xenoliths were also found. Textures show no correlation with mineral chemistry.

Harzburgite 3896 from Nidda is similar to the protogranular harzburgite 3816 from Dreihausen. Olivine has Fo content between 91.3 and 91.7 %. Orthopyroxene (Mg# 0.92) is Al-poor, having 0.10 atoms of Al pfu, and spinel is Cr-rich (Cr# 0.57).

The remaining harzburgites and lherzolites from Nidda are partly similar to the deformed Dreihausen xenoliths. Olivine exhibits a slightly wider range of Fo (89.3 to 91.7 %). Pyroxenes have Mg# corresponding to that of olivine and Al content of 0.12-0.23 atoms pfu (orthopyroxene) and 0.17-0.28 atoms pfu (clinopyroxene). Most lherzolites contain aluminous spinel with Cr# 0.14-0.23, whereas spinel in harzburgites is more chromian (Cr# 0.29-0.51).

Pyroxenes in Nidda xenoliths also exhibit decoupling between major and trace element mineral chemistry, with the exception of harzburgite 3896. Orthopyroxene from this depleted harzburgite has a REE pattern similar to the sinusoidal one (type I) from Dreihausen. Orthopyroxene patterns from the rest of the suite are either similar to the spoon-like pattern of lherzolite 3809 (type II) from Dreihausen or show constant mild decrease of concentrations from HREE to LREE (Fig. 8). Patterns of clinopyroxenes coexisting with type II orthopyroxene are also spoon-like. The rest of the clinopyroxenes (together with those from dunite and pyroxenites) exhibit patterns that are similar either to type III or type IV of clinopyroxene from Dreihausen.

4.2 Massif Central xenolith suites

Both studied xenolith suites come from southern domain of Massif Central (Fig. 10). The xenoliths from Allègre are rounded to flattened, most often from few to 13 cm across. Those from Alleyras are up to 19 cm in size. They are mostly spinel lherzolites and scarce spinel harzburgites (Fig. 11). The textures of spinel lherzolites are mostly porphyroclastic to equigranular, with a variation in the grain size from sample to sample (Fig. 12). The harzburgites are protogranular (Fig. 12), and sample 3763 from Alleyras has slightly larger olivine grains than harzburgite 3792 from Allègre. The xenoliths from these two sites, despite occurring 30 km apart, exhibit similar variation of chemical composition of minerals and their trace element characteristics.

The lherzolites contain olivine of Fo 89.5 - 90.6 % (Fig. 13), orthopyroxene of Mg# 0.897-0.910 with 0.12-0.15 atoms of Al pfu (Fig. 14), clinopyroxene of Mg# 0.894-0.916 with 0.20-0.29 atoms of Al pfu (Fig. 14) and aluminous spinel (Cr# 0.09-0.15; Fig. 13). Harzburgites contain olivine of Fo 90.7 - 91.1 % (Fig. 13), orthopyroxene of Mg# 0.913-0.914 with 0.08-0.09 atoms of Al pfu (Fig. 14), clinopyroxene of Mg# 0.915 with 0.13-0.15 atoms of Al pfu (Fig. 14) and Al-poor spinel (Cr# 0.45-0.46; Fig. 13).

The clinopyroxene REE contents are slightly (1-10x) enriched relative to primitive mantle. The REE patterns are flat with respect to MREE/HREE parts. Those of harzburgites are LREE-enriched (Fig. 15, patterns depicted “H”), whereas those of lherzolites are LREE-depleted (Fig. 15, patterns depicted “L1” and “L2”, depending on the degree of depletion). The harzburgite clinopyroxenes exhibit well defined HFSE negative anomalies in the trace element patterns (Fig. 15 c), whereas the lherzolitic ones exhibit a shallow negative Ti anomaly and lack the Zr-Hf one (Fig. 15

d, e). Orthopyroxene REE and trace element patterns show that harzburgites (H) are significantly different from the L1 and L2 lherzolites, which have similar orthopyroxene patterns (Supplementary material 6).

4.2.1. Microstructure and crystallographic preferred orientation

The lherzolitic xenoliths from Allègre show two types of olivine crystallographic preferred orientations (CPO, Fig. 16). The first type (samples 3797, 3790) is characterized by a strong concentration of [100] axes marking the lineation and [010] axes parallel to pole of the foliation. The second type (samples 3788, 3795) is characterized by almost complete girdles on [100] and [001] axes within the foliation plane, and a strong concentration of [010] axes parallel to the pole of the foliation. All analysed lherzolites from Alleyras (except sample 3763) show olivine CPO similar to the second type from Allègre, but with a slightly stronger olivine fabric (mud 4.75 - 5.81 and J-index 3.21 – 3.50, compared to mud 3.06 - 3.62 and J-index 2.82-3.27 in lherzolite from Allègre; Fig. 16). In Alleyras lherzolites, a slightly stronger fabric is illustrated by olivine [100] and [001] axes showing incomplete girdles within the foliation plane and a strong concentration of [010] parallel to pole of the foliation. However, harzburgite 3763 from Alleyras records the strongest olivine CPO (J-index 5.63) in this xenolith suite. The three axes indicate strong concentrations, with [100] axes parallel to the determined lineation, [010] perpendicular to the foliation plane and [001] within the foliation plane (parallel to Y; Fig. 16). Harzburgite 3792 from Allègre shows a fabric similar to the first lherzolite type, showing a strong concentration of [100] axes marking the lineation and [010] axes parallel to the pole of the foliation.

From both sites and all samples, the orthopyroxene fabrics are characterized by a point concentration of [001] parallel (3797, 3790, 3762, 3763, 3764), or at a slight angle (3792, 3788, 3795, 3748) to olivine [100] axes (Fig. 16). Nevertheless, a difference is noticeable between orthopyroxene CPO from harzburgite and lherzolites from Alleyras. Orthopyroxene [010] axes from the Alleyras harzburgite form a strong concentration point perpendicular to the observed foliation plane, while in lherzolitic samples the [100] orthopyroxene axes are perpendicular to the observed foliation plane and in many samples [100] and [010] form girdles (Fig. 16).

In all lherzolitic samples, clinopyroxene CPO show weaker fabrics than orthopyroxene and olivine, and it is sometimes difficult to determine the plane of dislocation glide. However, clinopyroxene [001] axes indicate concentration points always parallel to orthopyroxene [001] axes and olivine [100] axes (Fig. 16).

5. Discussion

5.1. Vogelsberg

The peridotite xenolith suites from both Vogelsberg localities are similar in their textures and major element chemical composition. Both suites are dominated by variously deformed peridotites which contain Al-rich spinel and pyroxenes. Protogranular harzburgite samples containing Cr-rich spinel, no/little clinopyroxene and Al-poor orthopyroxene are scarce.

Pyroxenes and spinel in the deformed rocks are enriched in Al relative to the protogranular harzburgites, indicating that the metasomatic event was synkinematic. Spinel forms streaks parallel to the foliation or is grouped in domains of reduced grain-size (Fig. 5), which suggests that deformation and metasomatism led to spinel recrystallization. The Cr# of spinel is linearly correlated with Al content of ortho- and

clinopyroxene (Supplementary material 5), indicating that these silicate phases were also affected by the same metasomatic event, although the spatial arrangement of their grains is not as obvious as that of spinel.

The protogranular harzburgite 3816 is the most depleted lithology in the mantle beneath Dreihausen. Its olivine is Fo 91.3, orthopyroxene is Al-poor, its spinel is chromian (Cr# 0.57) and it contains no detectable clinopyroxene. HREE content in its orthopyroxene is significantly lower than in orthopyroxene from other peridotites of this suite. This is the only rock containing orthopyroxene characterised by negative Ti and Hf anomalies. These characteristics suggest that harzburgite 3816 comes from mantle which was subjected to significant melt extraction. The absence of clinopyroxene points to high a degree of partial melting, since this mineral disappears at ~ 25% partial melting (e.g. Walter 1998). Negative Ti, Zr and Hf anomalies indicate that, after clinopyroxene consumption, further partial melting took place with orthopyroxene on the solidus. The LREE-enriched REE pattern of orthopyroxene shows that it was later slightly affected by metasomatism (Fig. 9).

The remaining peridotites from Dreihausen contain orthopyroxene significantly richer in HREE and Al, which suggests that they have been metasomatised by melts which affected major, LREE and HREE mineral compositions. To understand the relationship of the metasomatising melts to the lavas of Vogelsberg, we have calculated the REE patterns and Zr/Nb ratios of hypothetical melts in equilibrium with both clino- and orthopyroxene (Electronic Supplementary material 7). For REE ratios we used partition coefficients of Yao et al. (2012), whereas for Zr and Nb those of Hart and Dunn (1993) were used.

As a reference we used the averages of four major groups of lavas from Vogelsberg: (1) high-Ti basanites, (2) tholeiites, (3) olivine tholeiites and (4) alkali

basalts. Our grouping of these rocks is different from that proposed by Bogaard and Wörner (2003) except for high-Ti basanites. We classified the lavas as tholeiites/olivine tholeiites/alkali basalts based on their CIPW norm and following the scheme of Yoder and Tilley (1962). This enabled us to distinguish between silica-undersaturated lavas (not able to precipitate orthopyroxene), silica-saturated (able to precipitate orthopyroxene) and silica-oversaturated (able to precipitate orthopyroxene by reaction with olivine). We excluded lavas with high (>5 wt. %) normative quartz from the tholeiite group as potentially contaminated by crustal material.

When compared with the natural lavas, the hypothetical melts:

(1) calculated from types II and III orthopyroxene and clinopyroxene compositions have REE patterns different from those of any kind of Vogelsberg lava (Electronic Supplementary material 7);

(2) calculated from type IV orthopyroxene compositions have REE patterns similar to those of alkali basalt/high-Ti basanite/olivine tholeiite. The exception is harzburgite 3831, which has a REE pattern of similar shape, but shifted to slightly lower element abundances (Electronic Supplementary material 7);

(3) calculated from type IV clinopyroxene compositions have REE patterns similar to those of alkali basalt/high-Ti basanite/olivine tholeiite, but shifted to slightly higher element abundances (Electronic Supplementary material 7).

The differences between melts calculated from type IV ortho- and clinopyroxene may be the result of disequilibrium between the phases or of the partition coefficients which do not perfectly reproduce the real system. In order to investigate trace element equilibria between ortho- and clinopyroxene, we calculated the hypothetical clinopyroxene REE composition using the measured orthopyroxene REE one and partition coefficients of Lee et al. (2007). In most cases the calculated REE pattern

for 1200 ºC has a shape identical to those of real clinopyroxenes, but is slightly displaced below them in the diagram. The calculated REE pattern for 1400 ºC has a shape deviating in its LREE part from that of real clinopyroxenes, and is displaced above them in the diagram. Lherzolites 3817 and 3824 yield calculated patterns differing from the real ones, suggesting REE disequilibrium between ortho- and clinopyroxene.

The lavas of Vogelsberg differ in their Zr/Nb ratios: the high-Ti basanites and tholeiites have significantly higher Zr/Nb ratios than the basanites (Bogaard and Wörner 2003). This is also visible when the rocks are grouped according to our classification (see above). The average Zr/Nb ratios are 4.45 for high-Ti basanites, 6.07 for tholeiites and 2.99 for alkali basalts. The Zr/Nb ratios of hypothetical melts calculated from clinopyroxene compositions are 0.52 for type II, 3.35 for type III, 11.27 for type IV sample 3811, 6.13 for sample 3833 and websterite 3814 and 3.12 for sample 3842. These values might suggest that type II was not metasomatised by lavas which form the Vogelsberg volcano, whereas type III could have been metasomatised by alkali basalts or high-Ti basanites, but was subsequently affected by another metasomatic episode which increased its LREE contents. The latter involved a metasomatic agent richer in LREE than alkali basalts. Type IV xenoliths were affected by melts with REE patterns similar to alkali basalts (Supplementary material 7), but the high Zr/Nb ratios are not consistent with this kind of metasomatism. These relations suggest that the metasomatism was polyphase. The high Zr/Nb ratios as well as high orthopyroxene content in some samples (cf. Fig. 4) suggest that tholeiitic metasomatism (i. e. percolation of melts able to react with olivine and replace it by orthopyroxene) occurred beneath Vogelsberg. Subsequent cryptic metasomatism by alkali basalts possibly changed the trace element contents

in pyroxenes, but did not affect the major element compositions of phases. This possibly also explains the decoupling between major and trace element systematics of Vogelsberg peridotites.

Lithosphere thinning and asthenosphere upwelling led to long-lasting (18.0 – 14.7 Ma), compositionally evolving volcanism (Bogaard and Wörner 2003) related to rifting in the Vogelsberg. Abundant deformed mantle xenoliths suggest that rifting induced deformation in the stretching lithospheric mantle. The zones of high deformation enabled reactive melt migration, producing peridotites of variable composition. The lithospheric mantle underlying Vogelsberg is therefore heterogeneous. It shows no obvious relationship with the overlying crustal units: the major geological units in the upper crust of Vogelsberg seem to be decoupled from the SCLM. The implication is that the major boundaries of the Variscan orogen did not exert significant control on processes occurring in the underlying lithospheric mantle.

5.2. Massif Central

The harzburgites are characterized by relatively high Mg#s of olivine (ca. Fo 91, Fig. 13), pyroxenes (Mg# 0.91 – 0.92) low Al contents (Fig. 14) and Cr-rich spinel (Fig. 13). The clinopyroxene REE patterns are LREE-enriched, the trace-element patterns have well defined HFSE anomalies (Fig. 15). In contrast, the lherzolites (Fig. 13) contain less magnesian olivine (ca Fo 89-90) and higher-Al pyroxenes (Figs. 13 and 14), and Al-rich spinel (Fig. 13). The clinopyroxene trace element patterns are LREE-depleted, without strong Ti, Zr and Hf anomalies (Fig. 15). The xenolith suites from Allègre and Alleyras described in this paper correspond well to earlier descriptions of lithospheric mantle variation beneath the Massif Central (Gu et al. 2016, Downes et al.2003, Lenoir et al. 2000; Zangana et al. 1997, 1999). A detailed

trace element data set by Uenver-Thiele et al. (2017) distinguished three kinds of clinopyroxene REE patterns in the southern domain of the Massif Central. Their pattern A corresponds to the lherzolitic one described by us, whereas their patterns B and C correspond to those in harzburgites. Uenver-Thiele et al. (2017) showed that some samples contain clinopyroxene with variable REE patterns showing a transition from A to B patterns defined by them.

Both literature and our data show that the southern domain of the Massif Central is dominated by rocks of lherzolite composition which are relatively fertile in terms of major element contents (Figs. 13, 14). They are much more abundant than harzburgites, which are characterized by depletion in major elements, and contain LREE-enriched clinopyroxene.

A set of data largely identical to those from Allègre or Alleyras was presented by Zangana et. al. (1997, 1999), who studied the xenolith suite from Ray Pic in the southern domain of the Massif Central. The xenolith suite from Ray Pic is dominated by lherzolites. The clinopyroxene REE variation is identical to that from Allègre or Alleyras (for diagrams see Electronic Supplementary Material 8), although most of the analyses were done on clinopyroxene concentrates. LREE-depleted patterns typically occur in clinopyroxene-rich lherzolites, whereas LREE-enriched ones occur in clinopyroxene-poor lherzolites and harzburgites. The few exceptions may reflect that modal contents of minerals were calculated from chemical data, and some rocks contain clinopyroxene-rich patches/veins.

The study of olivine CPO reveals that fabric type is related to the site (Allègre or Alleyras), to the facies (lherzolite or harzburgite) and to the proportion of clinopyroxene. The first difference is seen in the harzburgite fabric from Alleyras and other samples. This harzburgite shows the strongest fabric (J-index= 5.64), which

suggests activation of [100](010) A-type slip system (A-type defined by Jung et al. 2006). The harzburgite from Allègre, despite a weaker fabric, also indicates activation of the olivine A-type slip system (Fig. 16). Olivine A-type system is classically considered to operate in the upper mantle under high temperature and low stress, in dry conditions (Nicolas et al. 1971, Ben Ismail and Mainprice 1998, Karato 2008). The olivine CPO type identified in Allègre lherzolites with a low proportion of clinopyroxene (5 and 6 % of clinopyroxene in samples 3797 and 3790, respectively) also shows the activation of the olivine A-type slip (Table 2, Figs. 11 and 16). All other lherzolites from Allègre or Alleyras analysed with EBSD (samples 3788, 3795, 3748, 3762, 3764) contain a higher proportion of clinopyroxene (11 – 15.6 %, Table 2, Fig. 11) and show the possible A-type fabric evolution toward an axial [010] fabric (also referred to AG-fabric by Mainprice 2003 or A/B-type by Précigout and Hirth, 2014). The olivine axial [010] fabric is known to be activated by axial shortening (Tommasi et al. 1999), or in the presence of melt in focused shear bands (Holtzman et al. 2003, Kohlstedt and Holtzman, 2009) or as a transient fabric between A- and B-type (Sundberg and Cooper, 2003). However, in natural samples axial [010] fabric developed during axial shortening is characterized by a stronger orientation of [100] than [001] (Tommasi et al. 1999), which is not obvious in Alleyras and Allègre xenoliths. The variable formation of axial [010] fabric in these xenoliths could be related to the presence of melt and/or to a change in the slip system.

In Alleyras harzburgite, the concordant deformation of orthopyroxene with olivine is shown by the major activation of [001](010) slip system (Fig. 16). The orthopyroxene [001](010) slip system has been identified in experimental conditions at high temperature (> 1000°C) with wet polycrystalline aggregates for a strain greater than 40% (Ross and Nielsen, 1978), or for temperature varying between 800

and 1100C°, for compressional strain from 11 to 28% (Ohuchi et al. 2010), and in natural rocks at temperature between 950 and 1000°C, estimated strain at 10-12 s^{-1} and variable hydration conditions (Frets et al. 2012).

The orthopyroxene of Allègre harzburgite and lherzolites indicate a strong ABC-type (or [001]{0kl} after Jung et al. 2010), except for sample 3788 which shows a stronger [001](010) fabric (as in Alleyras harzburgite). Orthopyroxene ABC-type has been first described in 2010 (Jung et al.) with a sample containing 17% of orthopyroxene deformed at 850-1000°C, 7-11kb, and 10-20 MPa stresses conditions (Jung et al. 2009). In lherzolites from Alleyras, the orthopyroxene fabrics of two samples (3748, 3762) are consistent with activation of orthopyroxene [001](100) slip. Orthopyroxene [001](100) slip is the most commonly activated slip in orthopyroxene, for high to moderate temperature in both natural rocks and experiments, at lithospheric conditions (Ross and Nielsen, 1978; Ohuchi et al. 2010; Mackwell, 1991). Amongst 9 samples, three orthopyroxene CPO are observed, with no clear relationship with the type of peridotite. Conditions required to activate these slip systems are variable, and not well constrained by this study, however the deformation recorded by these xenoliths occurred at high temperature (e.g. Alleyras harzburgite at 900-920°C using the Brey and Köhler, 1990, thermometer).
In xenoliths from both sites, from harzburgite to lherzolites (with cpx > 11%), the olivine fabric changes from a strong A-type through weaker A-type to axial [010] (Fig. 16). The evolution of olivine fabric is coherent with the increasing proportion of clinopyroxene, and the decrease of olivine and orthopyroxene Mg#.

These relationships between harzburgites and lherzolites, with an increase in clinopyroxene proportion, are similar both in terms of mineral chemistry and fabric evolution to those seen in the Lherz massif (French Pyrénées), where harzburgitic

mantle was refertilised and replaced by lherzolite (Le Roux et al. 2007). Bearing in mind that mantle xenoliths do not allow examination of outcrop-scale structural relationships, the study of microstructure suggests that consideration of insights from orogenic massifs can provide useful analogues for data interpretation. If so, diffuse melt percolation will affect the primary deformation (reheating) and will promote recovery (annealing) that will reduce the number of low-angle boundaries and will form 120° triple junctions, which occurred in olivine grains from harzburgitic to lherzolitic samples (with a high proportion of clinopyroxene; Fig. 17). Moreover, the almost undeformed and small disseminated clinopyroxene grains confirm the refertilised character of the lherzolite (Fig. 17). Some samples, even with a high proportion of undeformed clinopyroxene grains (e.g. 3748, 3764) show a distinct concentration of [001] axes parallel to the lineation (Fig. 16), which could formed by diffusion creep (e.g. Sundberg and Cooper, 2008, Précigout and Hirth, 2014). The development of clinopyroxene weak CPO and olivine axial [010] in lherzolite with a high proportion of clinopyroxene suggests that deformation was still active during melt percolation.

Our interpretation is thus opposite to those presented previously, which assumed that (1) lherzolites of the southern domain were affected by partial melting with a slight metasomatic overprint in places, and (2) harzburgites document stronger melt depletion overprinted by stronger, multiple metasomatism. A recent review of this kind of interpretation is given in Uenver-Thiele et al. (2017). In contrast, our analysis suggests that lherzolites are the result of metasomatic refertilisation of harzburgites, and the Lherz massif in the Pyrénées offers an analogue model of relationships between lherzolites and harzburgites in the lithospheric mantle beneath the southern domain.

The composition of olivine is mostly richer in forsterite than that of the DMM proposed by Workman and Hart (2005; cf. Fig. 14). Orthopyroxene is impoverished in Al and REEs relative to that of DMM (see Fig. 14 and Supplementary material 6). On the other hand, clinopyroxene Mg# values, Al contents and REE contents, as well as the Cr# and Mg# of spinel, are similar to those of the model DMM (Workman and Hart 2005). In our opinion these relationships mirror the nature of metasomatism: a strongly depleted harzburgitic protolith was modified by addition of clinopyroxene ("stealth metasomatism by O'Reilly and Griffin, 2013, implying addition of minerals that previously formed part of the assemblage), whereas pre-existing olivine and orthopyroxene were subjected to continuous exchange reactions lowering their Mg# and increasing Al contents, which advanced to different degrees. Spinel, which occurs in harzburgites, reacted completely Thus, olivine and orthopyroxene have "mixed" (protolithic and metasomatic) characteristics, whereas clinopyroxene and spinel are purely metasomatic (assuming that clinopyroxene did not re-equilibrate its composition with the olivine and orthopyroxene).

The harzburgites from both domains represent the depleted protolith, affected by various kinds of metasomatism (Uenver-Thiele et al., 2017). Harzburgites in the SCLM beneath the northern Massif Central are similar to those beneath Lower Silesia. The northern "depleted" domain of the Massif Central possibly represents the "orogenic mantle" similar to the Lower Silesian one. The Massif Central SCLM was formed in the Variscan collision zone at the margin of Gondwana. The northern domain escaped later metasomatism which could be strong enough to obliterate orogenic fingerprints, whereas the southern domain was subjected to strong refertilisation. It is an open question when the refertilization took place. It could have occurred during late orogenic Variscan delamination and asthenosphere upwelling

connected with decompression melting followed by cooling. This is suggested by a ca. 280 Ma thermal event in the lower crust, inducing zircon growth in granulite xenoliths from Bournac in the southern domain (Rossi et al. 2006). The ultrabasic/basic intrusion at the Moho documented by xenoliths from Puy Beaunit (northern domain) was dated at 257 ±6 Ma (Féménias et al. 2003). However, this intrusion (1) exhibits enrichment in LREE and LILE, which suggests that it is not related with DM mantle upwelling described in the southern domain and (2) is located in the northern mantle domain. Therefore, it cannot be unambiguously related to the refertilization of the southern domain. Alternatively, the discussed refertilization could be the result of Meso-/Cenozoic rifting. Further work is required to pinpoint the timing of the massive lithospheric mantle overprint documented in the region and to further test the various hypotheses on the regional mantle evolution.

5.3. A comment on Lower Silesia SCLM

The SCLM beneath Lower Silesia in SW Poland forms a distinct, well characterized domain in the mantle roots of European Variscan orogen (Puziewicz et al. 2015). Here we summarize the most important findings and comment on the nature of Lower Silesian SCLM, which is necessary for orogen-scale synthesis.

The xenolith suites of Lower Silesia are dominated by harzburgites (Electronic Supplementary Material 9, Fig. 1). Clinopyroxene-poor lherzolites are abundant in the Grodziec suite only (Matusiak-Małek et al. 2017a). Forsterite content in olivine allows to classify the xenoliths into two “groups”, referred to as A and B (Matusiak-Małek et al.2014, Puziewicz et al. 2015).

Xenoliths of group A contain olivine Fo 90.5 – 92.0, Al-poor orthopyroxene (Al typically 0.05 – 0.10 atoms pfu, Fig. 2, which corresponds to ca. 0.5 – 2.5 wt. %

Al_2O_3) and Cr-rich spinel (Electronic Supplementary Material 9, Fig. 2). Clinopyroxene, if present, is also Al-poor (Fig. 2). Scarce Cr-rich amphibole was noted (Matusiak-Małek et al. 2017b). Clinopyroxenes in harzburgites are typically impoverished in trace elements and REEs relative to primitive mantle, with the exception of LREE. Their REE patterns are LREE enriched, spoon- or U-shaped. The trace element patterns have deep negative Nb-Ta, Zr-Hf and Ti anomalies (Electronic Supplementary Material 9, Fig. 3).

The xenoliths of group B contain olivine Fo 84.0 – 90.0, Al-poor orthopyroxene (Al content similar to that of group A) and clinopyroxene, and Mg# of both correspond to that of coexisting olivine (Electronic Supplementary Material 9, Fig. 2). Clinopyroxenes in harzburgites are typically enriched in trace elements and REEs relative to primitive mantle. Their REE patterns exhibit an increase from HREE to LREE with an inflection at the LREE. Trace element patterns have shallow negative Nb-Ta, Zr-Hf anomalies, and a pronounced Ti anomaly (Electronic Supplementary Material 9, Fig. 3).

The B harzburgites were divided into two “subgroups” (Puziewicz et al. 2016). Group B1 containing Al-poor orthopyroxene (typically 0.05 – 0.10 atom of Al pfu) irrespective of the forsterite content of coexisting olivine (Electronic Supplementary Material 9, Fig. 2). The B2 harzburgites contain orthopyroxene with Al content up to 0.24 atoms pfu (corresponding to ca 5.7 wt. % Al_2O_3), negatively correlated with forsterite contents of coexisting olivine.

The xenoliths occur in lavas which erupted at 30-32 Ma (Steinberg, Księginki, Pilchowice), at 18-22 (Krzeniów, Wilcza Góra, Pilchowice) Ma and at 4 Ma (Lutynia). Two suites hosted by ca 30 Ma lavas (both nephelinites) represent mantle sections which have been heated to 1000 – 1100 ºC (Księginki 1100 – 1120 ºC, Puziewicz et

al. 2011; Grodziec 1010-1120 ºC, Matusiak-Małek et al. 2017). The xenoliths occurring in the of 18-23 Ma old lavas were entrained from mantle parts with temperatures varying in the range 880-1045 ºC (Wilcza Góra – Matusiak-Małek et al. 2017) or were not thermally equilibrated due to locally varying advective heat input (Krzeniów – Matusiak-Małek et al. 2014, Pilchowice – Ćwiek et al. 2018).

The harzburgites of group A have been subjected to 20 – 30 % melting (Matusiak-Małek et al. 2014, 2017a, b; Kukuła et al. 2015; Ćwiek et al. 2018). Subsequently these rocks have been metasomatised by carbonated silicate melts which added clinopyroxene (Puziewicz et al. 2015 and references therein).

The pre-metasomatic features of those harzburgites comprise high Fo olivine (90.5 to 92.0) and strong Al-depletion in orthopyroxene (commonly 0.05 – 0.10 atoms pfu, rarely up to 0.13 atoms of Al pfu). Aluminium poor orthopyroxene is characteristic for (1) MORB-source oceanic mantle formed in mid-ocean ridges ("abyssal" mantle) and (2) mantle wedge affected by extreme melting in supra-subduction zones (SSZ). The SSZ harzburgites usually contain Al-poor orthopyroxene (< 2.0 wt. % Al_2O_3) compared to those of the abyssal peridotites (2.5 – 4. 0 wt. % Al_2O_3; Bonatti and Michael 1989). However, there are exceptions from this simple relationship, e. g. the compilation of Arai and Ishimaru (2008) shows that primary orthopyroxene in SSZ settings contain up to 4 wt. % Al_2O_3 (Avacha and Iraya xenolith suites), and the Japanese xenoliths contain up to 7 wt. % Al_2O_3. The higher-Al orthopyroxene may occur because of involvement of abyssal peridotites in the SSZ settings (Arai and Kida 2000). Nevertheless, the SSZ and abyssal orthopyroxene Al_2O_3 contents overlap. Moreover, although the Al-impoverishment in orthopyroxene is basically due to melt extraction, the orthopyroxene composition is affected by other local factors like degree of melt extraction, composition of melts or fluids which react with

peridotite or temperatures of both processes (see e. g. Arai and Ishimaru 2008 for mantle wedge, Bodinier and Godard 2005 for abyssal peridotites). The olivine Fo is similar in both SSZ (90.0 – 92.5) and abyssal (89.6 – 92.2) peridotites (see e.g. compilation in Tollan et al., 2017) and therefore cannot serve as a criterion for their separation. Therefore, the low Al-orthopyroxene from the Lower Silesian mantle, when coupled with Fo contents of 90.5 to 92.0, suggest that Lower Silesian xenoliths come from fossil mantle wedge or from a slice of oceanic plate attached to it. This kind of tectonic setting occurs at the surface, where the Central Sudetic accretionary prism is considered to have originated during closure of the Variscan Ocean (Mazur et al. 2015).

The harzburgites of group B were formed by reactive basaltic melt percolation which lowered Mg# in olivine and orthopyroxene ("Fe metasomatism"; Puziewicz et al. 2015 and references therein). In B1 harzburgites this metasomatism did not affect the low Al content of orthopyroxene, and Puziewicz et al. (2016) speculated that the melt possibly was of a different composition and origin than that which produced the B2 harzburgites. The latter originated due to reactive alkaline basaltic melt percolation during Cenozoic rifting.

5.4. Synthesis and perspective: differences and similarities among the SCLM domains

Our study evidences significant differences among the SCLM occurring beneath various parts of the Variscan orogen in Europe. These differences are in part due to a metasomatic overprint of SCLM during Cenozoic rifting and volcanism. In Lower Silesia the pre-metasomatic protolith appears to be strongly depleted and characteristically Al-poor. We suggest that the SCLM beneath Lower Silesia is the

fossil Variscan mantle wedge possibly with a slice of oceanic mantle attached to it. The Lower Silesian SCLM is similar to the mantle underlying the northern domain of the Massif Central. The latter was also interpreted as originating in the suprasubduction setting (Gu et al. 2016 and references therein). Both of these depleted SCLM domains are located at the marginal parts of fossil Variscan terrains: Lower Silesia at the eastern termination of Saxo-Thuringian Zone, and the northern Massif Central at the northern margin of Gondwana.

The mantle domain beneath Vogelsberg is strongly metasomatically overprinted and its protolith features seem to be completely obliterated. Our study shows that the Cenozoic rifting which opened the Upper Rhine Rift resulted in deformation of the lithospheric mantle, and the prolonged, multi-phase volcanism led to multiple metasomatic events in the SCLM. Vogelsberg is located at the boundary between three major units of Variscan orogen: Rheno-Hercynian Zone, Northern Phyllite Zone and Mid-German Crystalline High (Fig. 3). The two investigated xenolith suites in the present study are so strongly metasomatically overprinted that an assessment of potential differences between their protoliths is not possible. The Vogelsberg example shows that domains of strongly modified SCLM preserving no pre-rifting record occur in Cenozoic rifting zones in the European Variscan orogen.

The southern domain of the Massif Central offers another example of mantle which was intensely metasomatically overprinted. This metasomatism produced lherzolites at the expense of pre-existing harzburgites. The lherzolites contain LREE-depleted clinopyroxene, which makes them unique compared with other SCLM domains described in this study. Refertilization of harzburgitic SCLM by melts able to produce clinopyroxene which is depleted in LREE relative to HREE suggests that the southern domain of the Massif Central was formed by late-orogenic asthenosphere

upwelling, which is envisaged in all models of Variscan orogen evolution. However, other processes are also possible (e. g. mantle which originated in MORB-source). The geodynamic context of the metasomatism which produced lherzolites of the southern domain therefore needs further studies.

Our study shows the existence of three kinds of SCLM, forming different "domains" of beneath the Variscan orogen. These domains are of size of tens to over hundred kilometres (Lower Silesia plus Upper Lusatia 80 km x 240 km, Vogelsberg 60 km x 60 km, southern domain of the Massif Central ca. 180 km x 110 km), but it remains an open question whether or not the described kinds of SCLM do occur beneath the whole Variscan orogen. The described SCLM types were formed by major processes operating during and after orogeny: (1) Lower Silesia – docking of incoming lithospheric plate to the growing orogen and subsequent weak mantle metasomatism at the peripheries of the continental rifting zones, (2) southern Massif Central – late orogenic replacement of delaminated orogenic mantle root by upwelled asthenosphere, and (3) Vogelsberg – strong metasomatic lithosphere modification during continental rifting. Therefore, we suggest that the SCLM beneath parts of Variscan orogen not described in this study consists of fragments which are similar to those we describe in the present study.

7. Conclusions

Xenolith-based studies using new and published data enable us to define three major kinds of European Variscan lithospheric mantle (Fig. 18). These are:

(1) *Variscan orogenic mantle*: mostly harzburgitic, depleted mantle overprinted by low intensity metasomatism by carbonated alkali basaltic melts. It represents mantle wedge and mantle slices docked to the wedge during collision. It forms the Lower

Silesian domain. This kind of mantle may also occur in the "northern domain" of the French Massif Central;

(2) *Cenozoic rifted mantle*: harzburgitic to lherzolitic mantle intensely reworked by silicate melt percolation related to Cenozoic rifting. It is not possible to recognize its protolith. It was modified by silica-saturated to oversaturated basaltic melts, which produced orthopyroxene-rich peridotites. Pre-eruptive overprint by alkali basaltic melts formed the REE/trace element characteristics of pyroxenes. This kind of mantle occurs beneath the Vogelsberg volcano in the Rhine Graben;

(3) *Asthenosphere-derived mantle*: lherzolite-dominated, refertilized mantle which represents a harzburgitic protolith reworked by melts coming from the upwelling asthenosphere in a process similar to that described from the Lherz massif in the Pyrénées (Le Roux et al. 2007). The lherzolites have chemical characteristics similar to or slightly more depleted than the Depleted MORB Mantle (DMM) of Workman and Hart (2005). This kind of mantle occurs beneath the southern domain of the French Massif Central.

In the lithospheric mantle peridotites investigated so far, the major element record of geological processes in mineral chemistry is commonly decoupled from the trace-element record in pyroxenes. The evolution of lithospheric mantle after the Variscan collision stage was independent of the major geological structures which form the crustal part of the orogen.

Acknowledgements

Funding: This study was possible thanks to the project *Subcontinental lithospheric mantle beneath Europe* of Polish National Centre for Science (UMO-2014/15/B/ST10/00095) to JP. Large part of the microprobe data were gathered

thanks to the series of Austrian-Polish projects (WTZ PL 08/2018, WTZ PL16). LA-ICP-MS data from French Massif Central were collected during visiting professorship of JP at the University of Toulouse (November 2016), and those from Vogelsberg during DAAD Fellowship of MZ at the University of Frankfurt.

We are grateful to Hilary Downes and two anonymous Reviewers for their thoughtful and detailed reviews, which helped us to improve the earlier version of the paper. We thank Alan Woodland (handling editor) for his insightful suggestions and comments, which inspired us to improve the presentation. We thank A. Proietti for help during EBSD measurements. We are grateful to Johannes Glickel GmbH & Co. KG for help during sampling in the Dreihausen quarry, Basaltwerk Nidda GmbH for help during sampling in the Nidda quarry and to Perrachon S.A. for help during sampling in the Ringue quarry.

References

Arai, S., Ishimaru, S., 2008. Insights into petrological characteristics of the lithosphere of mantle wedge beneath arcs through peridotite xenoliths: a review. Journal of Petrology 49, 665-695.

Arai, S., Kida, M, 2000. Origin of fine-grained peridotite xenoliths from Iraya volcano of Batan Island, Philippines: deserpentinization or metasomatism at the wedge mantle beneath an incipient arc? The Island Arc 9, 458-471.

Aulbach, S., Sun, J., Tappe, S., Höfer, H., Gerdes, A., 2017. Volatile-rich metasomatism in the cratonic mantle beneath SW Greenland: Link to kimberlites and mid-lithospheric discontinuities. Journal of Petrology 58, 2311-2338.

Babuška, V., Plomerová, J., 2006. European mantle lithosphere assembled from rigid microplates with inherited seismic anisotropy. Physics of the Earth and Planetary Interiors 158, 264-280.

Babuška, V., Fiala, J., Plomerová, J., 2010.Bottom to top lithosphere structure and evolution of western Eger Rift (Central Europe). International Journal of Earth Sciences 99, 891-907.

Bali, E., Szabó, C, Vaselli, O., Török, K., 2002. Significance of silicate melt pockets in upper mantle xenoliths from the Balaton-Balaton Highland Volcanic Field, Western Hungary. Lithos 61, 79-102.

Ben Ismaïl, W., Mainprice, D., 1988, An olivine fabric database: an overview of upper mantle fabrics and seismic anisotropy. Tectonophysics 296, 145-157.

Bodinier, J.-L., Godard, M., 2005. Orogenic, Ophiolitic, and Abyssal Peridotites. In: Holland, H.D., Turekian, K.K., Carlson, R.W. (Editors), Treatise on Geochemistry: The mantle and the core. Elsevier Pergamon, Amsterdam.

Bogaard, P., Wörner, G., 2003. Petrogenesis of basanitic to tholeiitic volcanic rocks from the Miocene Vogelsberg, Central Germany. Journal of Petrology 44, 569–602.

Bonatti, E., Michael, P. J., 1989. Mantle peridotites from continental rifts to ocean basins to subduction zones. Earth and Planetary Science Letters 91, 297-311.

Brey, G. P., Köhler, T., 1990. Geothermobarometry in four-phase lherzolites II. New thermobarometers and practical assessment of existing thermobarometers. Journal of Petrology 31, 1353-1378.

Büchner, J., Tietz, O., Viereck., L., Suhr, P., Abratis, M., van den Bogaard, P., (2015). Volcanology, geochemistry and age of the Lausitz Volcanic Field. International Journal of Earth Sciences 104, 2057-2083.

Bunge, H.-J., 1982. Texture Analysis in Materials Science: Mathematical Methods. Elsevier.

Coisy, P., 1977.Structure et chimisme des péridotites en enclaves dans les basaltes du Massif Central. Modeles géodynamiques du manteau supérieur. These, Universite de Nantes, 115 pp.

Ćwiek, M., Matusiak-Małek, M., Puziewicz, J., Ntaflos, T., 2018. Lithospheric mantle beneath NE part of Bohemian Massif and its relation to overlying crust: new insights from Pilchowice xenolith suite, Sudetes, SW Poland. International Journal of Earth Sciences 107, 1731-1753.

Ćwiek, M., Puziewicz, J., Matusiak-Małek, M., Ntaflos, T., Grégoire, M., 2018. The lithospheric mantle underlying Northern Hessian Depression – a xenolith study. Geophysical Research Abstracts – EGU General Assembly 2018, 20: EGU2018-14409.

Dèzes, P., Schmid, S. M., Ziegler, P. A., 2004. Evolution of the European Cenozoic Rift System: interaction of the Alpine and Pyrenean orogens with their foreland lithosphere. Tectonophysics 389: 1-33.

Deer, W. A., Howie, R. A., Zussman, J., 1992. An Introduction to the Rock-forming Minerals. Longman, 1-696.

Downes, H., 2001. Formation and modification of the shallow sub-continental lithospheric mantle: a review of geochemical evidence from ultramafic xenolith suites and tectonically emplaced ultramafic massifs of Western and Central Europe. Journal of Petrology 42, 233-250.

Downes, H., 1987. Tertiary and Quaternary volcanism in the Massif Central, France. In: Fitton, J. G., and Upton, B. G. J. (eds.), Alkaline Igneous Rocks. Geological Society Special Publication 30, 517-530.

Downes, H., Reichow, M. K., Mason, P. R. D., Beard, A. D., Thirlwall, M. F., 2003. Mantle domains in the lithosphere beneath the French Massif Central: trace element and isotopic evidence from mantle clinopyroxenes. Chemical Geology 200, 71-87.

Ehrenberg, K.H., Hickenthier H., 1985. Die Basaltbasis im Vogelsberg: Schollenbau und Hinweise zur Entwicklung der vulkanischen Abfolge. Geologische Jahrbuch Hessen 113, 97-135.

Féménias, O., Coussaert, N., Bingen, B., Whitehouse, M., Mercier J.-C. C., Demaiffe, D., 2003. et al. 2003. A Permian underplating event in late- to post-orogenic tectonic setting. Evidence from the mafic–ultramafic layered xenoliths from Beaunit (French Massif Central). Chemical Geology 199, 293-315.

Franke, W., 2014. Topography of the Variscan orogen in Europe: failed – not collapsed. International Journal of Earth Sciences 103, 1471-1499.

Frets, E., Tommasi, A., Garrido, C.J., Padrón-Navarta, J.A., Amri, I., Targuisti, K., 2012. Deformation processes and rheology of pyroxenites under lithospheric mantle conditions. Journal of Structural Geology 39, 138-157.

Gu, X., Deloule, E., France, L., Ingrin, J., 2016. Multi-stage metasomatism revealed by trace element and Li isotope distributions in minerals of peridotite xenoliths from Allègre volcano (French Massif Central). Lithos 264, 158-174.

Hart, S. R., Dunn, T., 1993. Experimental cpx/melt partitioning of 24 trace elements. Contributions to Mineralogy and Petrology 113, 1-8.

Henk, A., 1999. Did the Variscides collapse or were they torn apart?: A quantitative evaluation of the driving forces for postconvergent extension in central Europe. Tectonics 18, 774-792.

Holtzman, B. K., Kohlstedt, D. L., Zimmerman, M. E., Heidelbach, F., Hiraga, T. Hustoft, J. 2003. Melt segregation and strain partitioning: implications for seismic anisotropy and mantle flow. Science 301, 1227-1230.

Jochum, K. P., Weis, U., Stoll, B., Kuzmin, D., Yang, Q., Raczek, I., Jacob, D. E., Stracke, A., Birbaum, K., Frick, D. A., Günther, D., Enzweiler, J., 2011. Determination of reference values for NIST SRM 610 – 617 glasses following ISO guidelines. Geostandards and Geoanalytical Research 35, 397-429.

Jung, H., Park, M., Jung, S., Lee, J., 2010. Lattice preferred orientation, water content, and seismic anisotropy of orthopyroxene. Journal of Earth Science 21,555-568.

Jung, H., Katayama, I., Jiang, Z., Hiraga, T., Karato, S. I., 2006. Effect of water and stress on the lattice-preferred orientation of olivine: Tectonophysics 421, 1-22.

Karato, S. 2008. Deformation of Earth Materials: An introduction to rheology of solid Earth. Cambridge University Press, 474p.

Kearey, P., Klepeis, K. A., Vine, F. J., 2008. Global Tectonics, 3rd Edition. Wiley-Blackwell, 482 p.

Kohlsdedt, D. L., Holtzman, B. K., 2009. Shearing melt out of the Earth: An experimentalist's perspective on the influence of deformation on melt extraction. Annual Review of Earth and Planetary Sciences 37, 561-593.

Kroner, U., Romer, R. L., 2013. Two plates – Many subduction zones: The Variscan orogeny reconsidered. Gondwana Research 24, 298-329.

Kukuła, A., Puziewicz, J., Ntaflos, T., Grégoire, M., Ćwiek, M., Matusiak-Małek, M., 2018. Preliminary data on mantle xenoliths from Alleyras (Devès Volcanic Field, French Massif Central). 3rd European Mantle Workshop, Pavia (Italy) 26-28 June 2018, Abstract Book, 82.

Kukuła, A., Puziewicz, J., Hidas, K., Ntaflos, K., Matusiak-Małek, M., Milke, R., 2017. Petrology and deformation style of lithospheric mantle beneath the Heldburg Dike swarm (Central Germany) subset of Central European Volcanic Province. Geophysical Research Abstracts – EGU General Assembly 2017, 10: EGU2017-7227-1.

Kukuła, A., Puziewicz, J., Matusiak-Małek, M., Ntaflos, T., Büchner, J., Tietz, O., 2015. Depleted subcontinental lithospheric mantle and its tholeiitic melt metasomatism beneath NE termination of the Eger Rift (Europe): the case study of the Steinberg (Upper Lusatia, SE Germany) xenoliths. Mineralogy and Petrology 109, 761-787.

Ladenberger, A., Michalik, M., Tomek, Č., Peate, D. W., 2006. Alkaline magmatism in SW Poland – An example of asthenosphere-lithoshere interactions? Mineralogia Polonica-Special Papers 29, 40-47.

Lee C.-T. A., Harbert A., Leeman W. P., 2007. Extension of lattice strain theory to mineral/mineral rare-earth element partitioning: An approach for assessing disequilibrium and developing internally consistent partition coefficients between olivine, orthopyroxene, clinopyroxene and basaltic melt. Geochimica et Cosmochimica Acta 71, 481-496.

Lenoir, X., Garrido, C., Bodinier, J. L., Dautria, J. M., 2000. Contrasting lithospheric mantle domains beneath the Massif Central (France) revealed by geochemistry of peridotite xenoliths. Earth and Planetary Science Letters 181, 359-375.

Lu, J., Zheng, J., Griffin, W. L., O'Reilly, S. Y., Pearson, N. J., 2015. Microscale effects of melt infiltration into the lithospheric mantle: Peridotite xenoliths from Xilong, South China. Lithos 232, 111-123.

Mackwell, S. J., 1991. High-temperature rheology of enstatite: implications for creep in the mantle. Geophysical Research Letters 18, 2027–2030.

Mainprice, D., 2009. Diffusion, deformation and mineral properties of the Earth's interior. Introduction. Physics of the Earth and Planetary Interiors 172, 3-4.

Martha, S., Zulauf, G., Dörr, W., Nesbor, H., Petschick, R., Prinz-Grimm, P., Gerdes, A., 2014. The Saxothuringian-Rhenohercynian boundary underneath the Vogelsberg volcanic field: evidence from basement xenoliths and U-Pb zircon data of trachyte. German Journal of Geology (Z. Dt. Ges. Geowiss.) 165, 373–394.

Matusiak-Małek, M., Ćwiek, M., Puziewicz, J., Ntaflos, T., 2017a. Thermal and metasomatic rejuvenation and dunitization in lithospheric mantle beneath Central Europe - The Grodziec (SW Poland) case study. Lithos 276, 15-29.

Matusiak-Małek, M., Puziewicz, J., Ntaflos, T., Grégoire, M., Kukuła, A., Wojtulek, P., 2017b. Origin and evolution of rare amphibole-bearing mantle peridotites from Wilcza Góra (SW Poland), Central Europe: xenolith suite case. Lithos 286-287, 302-323.

Matusiak-Małek, M., Puziewicz, J., Ntaflos, T., Grégoire, M., Benoit, M., Klügel, A., 2014. Two contrasting lithologies in off-rift subcontinental lithospheric mantle beneath Central Europe – the Krzeniów (SW Poland) case study. Journal of Petrology 55, 1799-1828.

Matusiak-Małek, M., Puziewicz, J., Ntaflos, T., 2013. Origin of intergranular aggregates in mantle xenoliths from Krzeniów basanite. Geoscience Notes 1, 25-49.

Matusiak-Małek, M., Puziewicz, J., Ntaflos, T., Grégoire, M., Downes, H., 2010. Metasomatic effects in the lithospheric mantle beneath the NE Bohemian Massif: A case study of Lutynia (SW Poland) peridotitic xenoliths. Lithos 117, 49-60.

Mazur, S., Turniak, K., Szczepański, J., McNaughton, N. J., 2015. Vestiges of Saxothuringian crust in the Central Sudetes, Bohemian Massif: Zircon evidence of a recycled subduction slab provenance. Gondwana Research 27, 825-839.

McDonough, W., Sun, S., 1995. The composition of the Earth. Chemical Geology 120, 223–253.

Meier, T., Soomro, R. A., Viereck, L., Lebedev, S., Behrmann, J. H., Weidle, C., Cristiano, L., Hanemann, R., 2016. Mesozoic and Cenozoic evolution of the Central European lithosphere. Tectonophysics 692, 58-73.

Mercier, J. C. C., Nicolas, A., 1975. Textures and fabrics of upper–mantle peridotites as illustrated by xenoliths from basalts. Journal of Petrology 16, 454 - 487.

Michon, L., Merle, O., 2001. The evolution of the Massif Central rift: spatio-temporal distribution of the volcanism. Bulletin de la Societe Geologique de France 172, 201-211.

Nicolas, A., Bouchez, J.-L., Boudier, F., Mercier, J.-C. C., 1971. Textures, structures and fabrics due to solid state flow in some European lherzolites. Tectonophysics 12, 55-86.

Ohuchi, T. Karato, S-I. Fujino, K. 2010. Strength of single-crystal orthopyroxene under lithospheric conditions: Contributions to Mineralogy and Petrology 161, 961-975.

O'Reilly, S. Y., Griffin, W. L., 2013. Mantle Metasomatism. Harlov, D. E., Austrheim, H., eds., Metasomatism and the Chemical Transformation of Rock, Lecture Notes in Earth Sciences, Springer, 471-533.

Pécskay, Z., Birenmajer, K., 2013. Insight into the geochronology of Cenozoic alkaline basaltic volcanic activity in Lower Silesia (SW Poland) and adjacent areas. In: Büchner, J., Rapprich, V., Tietz, O. (Eds.), Basalt 2013 – Cenozoic Magmatism in Central Europe, Abstract & Excursion Guides, pp. 66-67.

Plomerová, J., Babuška, V., 2010. Long memory of mantle lithosphere fabric – European LAB constrained from seismic anisotropy. Lithos 120, 131-143.

Precigout, J., Hirth, G., 2014. B-type olivine fabric induced by grain boundary sliding. Earth and Planetary Science Letters 395, 231-240.

Puziewicz, J., Ntaflos, T., Grégoire, M., Ćwiek, M., Tsymbal, O., 2017. Preliminary data on petrology of peridotite xenoliths from Rochemonteix in French Massif Central. Mineralogia-Special Papers 47, 77.

Puziewicz, J., Matusiak-Małek, M., Ntaflos, T., Kukuła, A., Ćwiek, M., 2016. Oceanic provenance of lithospheric mantle beneath Lower Silesia (SW Poland) and two kinds of its "Fe-metasomatism". Geophysical Research Abstracts – EGU General Assembly 2016, 18, EGU2016-3778.

Puziewicz, J., Matusiak-Małek, M., Ntaflos, T., Grégoire, M., Kukuła, A., 2015. Subcontinental lithospheric mantle beneath Central Europe. International Journal of Earth Sciences 104, 1913–1924.

Puziewicz, J., Koepke, J., Grégoire, M., Ntaflos, T., Matusiak-Małek, M., 2011. Lithospheric mantle modification during Cenozoic rifting in Central Europe: Evidence from the Księginki nephelinite (SW Poland) xenolith suite. Journal of Petrology 52, 2107-2145.

Ross, J.V., Nielsen, K.C., 1978. High-temperature flow of wet polycrystalline enstatite. Tectonophysics 44, 233-261.

Le Roux, V., Bodinier, J.-L., Tommasi, A., Alard, O., Dautria, J.-M., Vauchez, A., Riches, A. J. V., 2007. The Lherz spinel lherzolite : Refertilized rather than pristine mantle. Earth and Planetary Science Letters 259, 599-612.

Sawicki, L., 1995. Geological map of Lower Silesia with adjacent Czech and German territories (without Quaternary deposits) 1:100000. Państwowy Instytut Geologiczny.

Seiberlich, C. K. A., Ritter, J. R. R., Wawerzinek, B., 2013. Topography of the lithosphere-asthenosphere boundary below the Upper Rhine Graben Rift and the volcanic Eifel Region, Central Europe. Tectonophysics 603, 222-236.

Shaw, C. S. J., Klügel, A., 2002. The pressure and temperature conditions and timing of glass formation in mantle-derived xenoliths from Baarley, West Eifel, Germany: the

case for amphibole breakdown, lava infiltration and mineral-melt reaction. Mineralogy and Petrology 74, 163-178.

Sissingh, W., 2006. Syn-kinematic palaeographic evolution of the West European Platform: correlation with Alpine plate collision and foreland deformation. Netherlands Journal of Geosciences – Geologie en Mijnbouw 85, 131-180.

Sundberg, M., Cooper, R.F., 2008. Crystallographic preferred orientation produced by diffusional creep of harzburgite: effects of chemical interactions among phases during plastic flow. Journal of Geophysical Research 113, B12208, http://dx.doi.org/10.1029/ 2008JB005618.

Tollan, P. M., E., Dale, C. W., Hermann, J., Davidson, J. P., Arculus, R. J., 2017. Generation and modification of the mantke wedge and lithosphere beneath the West Bismarck Arc : Melting, metasomatism and thermal history of peridotite xenoliths from Ritter Island. Journal of Petrology 58, 1475-1510.

Tommasi, A. Tikoff, B., Vauchez, A., 1999. Upper mantle tectonics: Three-dimensional deformation, olivine crystallographic fabrics and seismic properties. Earth and Planetary Science Letters 168, 173-186.

Uenver-Thiele L., Woodland A. B., Seitz H.-M., Downes H., Altherr, R., 2017. Metasomatic processes revealed by trace element and redox signatures of the

lithospheric mantle beneath the Massif Central, France. Journal of Petrology 58, 395-422.

Uenver-Thiele, L., Woodland, A. B., Downes, H., Altherr, R., 2014. Oxidation state of the lithospheric mantle below the Massif Central, France. Journal of Petrology 55, 2457-2480.

Ulrych, J., Dostal, J., Adamovič, J., Jelínek, E., Špaček, P., Hegner, E., Balogh, K., 2011. Recurrent Cenozoic volcanic activity in the Bohemian Massif (Czech Republic). Lithos 123, 133-144.

Ulrych, J., Pivec, E., Lang, M., Balogh, K., Kropáček, V., 1999. Cenozoic intraplate volcanic rock series of the Bohemian Massif: a review. Geolines 9,123–129.

van Achterberg, E., Ryan, C. G., Jackson, S. E., Griffin, W. L., 2001. Data reduction software for LA-ICP-MS. In: Sylvester, P. J. (ed.) Laser ablation ICPMS in the earth sciences, Principles and Applications. *Mineralogical Association of Canada, Short Course Series* 29, 239–243.

Walter, M. J., 1998.Melting of garnet peridotite and the origin of komatiite and depleted lithosphere. Journal of Petrology 39, 29-60.

Wilson, M., Downes, H., 1990. Tertiary-Quaternary extension-related alkaline magmatism in Western and Central Europe. Journal of Petrology 32, 811-849.

Wimmenauer, W., 1974. The alkaline province of Central Europe and France. In: Sørensen, H., (ed.), The alkaline rocks. Wiley, London, pp 286-291.

Witt-Eickschen, G., (1993). Upper mantle xenoliths from alkali basalts of the Vogelsberg, Germany: implications for mantle upwelling and metasomatism. European Journal of Mineralogy 5, 361–376.

Workman, R. K., Hart, S. R., 2005. Major and trace element composition of the depleted MORB mantke (DMM). Earth and Planetary Science Letters 231, 53-72.

Yao, L., Sun, Ch., Liang, Y., 2012. A parameterized model for REE distribution between low-Ca pyroxene and basaltic melts with applications to REE partitioning in low-Ca pyroxene along a mantle adiabat and during pyroxenite-derived melt and peridotite interaction. Contributions to Mineralogy and Petrology 164, 261-280.

Yoder, H. S., Tilley, C. E., 1962. Origin of basalt magmas: An experimental study of natural and synthetic rock systems. Journal of Petrology 3, 342-532.

Zangana, N. A., Downes, H., Thirlwall, M. F., Marriner, G. F., Bea, F. 1999. Geochemical variation in peridotite xenoliths and their constituent clinopyroxenes from Ray Pic (French Massif Central): implications for the composition of the shallow lithospheric mantle. Chemical Geology 153, 11-35.

Zangana, N. A., Downes, H., Thirlwall, M. F., Hegner, E., 1997. Relationship between deformation, equilibration temperatures,REE and radiogenic isotopes in mantle

xenoliths (Ray Pic, Massif Central, France): an example of plume-lithosphere interaction? Contributions to Mineralogy and Petrology 127, 187-203.

Ziegler, P., Dèzes, P., 2005. Evolution of the lithosphere in the area of the Rhine Rift System. International Journal of Earth Sciences 94, 594-614.

Figure captions

Fig. 1. Occurrences of Cenozoic volcanic rocks relative to Variscan basement in central Europe. Volcanic rocks after Büchner et al. (2014), basement after Franke (2014), map compiled by Michał Dajek. LS – Lower Silesia, ER – Eger Rift, V – Vogelsberg, MC – Massif Central.

Fig. 2. Occurrences of Cenozoic alkaline volcanic rocks in SW Poland and neighbouring areas of Germany and Czech Republic (compiled by Michał Dajek and Danuta Lipa, University of Wrocław, on the basis of the "Geological map of Lower Silesia 1:100000" by Sawicki 1995). The inset in the right corner shows the location of the Eger Rift relative to Variscan basement of the Bohemian Massif after Ulrych et al. (1999). Thick green lines – sutures between Central Sudetes, Saxo-Thuringia (to the west) and Brunia/Avalonia (to the east) according to Mazur et al. (2015). Brunia/Avalonia in the depicted area corresponds to the Moravo-Silesian Zone.

Fig. 3. (a) Occurences of Cenozoic basaltic rocks relative to Upper Rhine Rift (based on the map of Sissingh 2006); (b) Extent of the Vogelsberg Volcanic Field (after Martha et al. 2014) with location of major mantle xenolith occurrences. Variscan

basement: RH – Rheno-Hercynian Zone, NPZ – Northern Phyllite Zone, MGCH – Mid-German Crystalline High.

Fig. 4. Points representing peridotites from Dreihausen in the ol-opx-cpx diagram. Red cross marks mineral composition of DMM (Depleted MORB Mantle, Workman and Hart 2005).

Fig. 5. Textural variation of lherzolites from Dreihausen. (a) slightly deformed lherzolite 3824. Note linear arrangement of spinel (black); (b) porphyroclastic lherzolite 3841, spinel grains located in rock parts with reduced grain-size; (c) foliated lherzolite 3843; (d) porphyroclastic lherzolite 3828. Optical images, plane polarised light. Olivine (Ol) is white, orthopyroxene (Opx) creamy, clinopyroxene (Cpx) pale green and spine (Spl) – black.

Fig. 6. (a) Olivine compositions in Dreihausen xenoliths in diagram Fo – NiO, (b) Spinel compositions in diagram Cr# - Mg#

Fig. 7. Orthopyroxene (a) and clinopyroxene (b) compositions in diagrams Mg# - Al. Symbols are identical to those in Fig. 6.

Fig. 8. REE patterns of orthopyroxene (a - c) and clinopyroxene (d - f) from Dreihausen. Primitive mantle normalised (McDonough and Sun, 1995) averaged multiple analyses in each sample.

Fig. 9. Trace element patterns of orthopyroxene (a - c) and clinopyroxene (d - f) from Dreihausen. Primitive mantle normalised (McDonough and Sun, 1995) averaged multiple analyses in each sample.

Fig. 10. Location of Allègre and Alleyras sites relative to Cenozoic volcanic rock occurrences in Massif Central.

Fig. 11. Points representing peridotites from Allègre and Alleyras in the ol-opx-cpx diagram. Red cross marks mineral composition of DMM (Depleted MORB Mantle, Workman and Hart 2005).

Fig. 12. Textural variation of peridotites from Allègre and Alleyras. (a) protogranular harzburgite 3763 from Alleyras; (b) fine-grained lherzolite 3764 from Alleyras, note interstitial location of spinel grains; (c) protogranular to porphyroclastic lherzolite 3788 from Allègre with abundant interstitial spinel; (d) equigranular lherzolite 3795 from Allègre. Optical images, plane polarised light. Olivine (Ol) is white, orthopyroxene (Opx) creamy, clinopyroxene (Cpx) pale green and spine (Spl) – black.

Fig. 13. (a) Allègre and (b) Alleyras olivine compositions in diagrams Fo – NiO. DMM = olivine of depleted MORB mantle after Workman and Hart (2005); (c) Spinel composition in diagram Cr# - Mg#.

Fig. 14. (a), (c) Allègre and (b), (d) Alleyras ortho- and clinopyroxene compositions in Mg# - Al diagrams. Symbols are identical to those in Fig. 11.

Fig. 15. REE (a, b) and trace element (c, d, e) patterns of clinopyroxenes from Allègre and Alleyras in Massif Central. Primitive mantle normalised (McDonough and Sun, 1995) averaged multiple analyses in each sample. Asterisks show DMM (Depleted MORB Mantle) orthopyroxene after Workman and Hart (2005).

Fig. 16. Crystallographic preferred orientations of olivine, orthopyroxene and clinopyroxene from Allègre and Alleyras xenoliths. Pole figures represent one point per grain on a lower-hemisphere, equal-area stereographic projection; n is the number of grains. For all pole figures, contours have been plotted at each multiple of the uniform distribution (md). The strength of the crystallographic preferred orientation (CPO) was estimated using the J-index (Bunge, 1982). The clinopyroxene (cpx) modal percentage is reported from Table 2.

Fig. 17. Misorientation (intracrystalline deformation) maps of olivine (A) from harzburgite to lherzolite with up to 15% of clinopyroxene. B) misorientation of clinopyroxene and C) orthopyroxene from a highly refertilised lherzolite 3762. The rainbow bar is the misorientation scale. The blue indicates a value close to the mean grain orientation, while red color indicates a deviation of 10° or more from the mean grain orientation.

Fig. 18. Preliminary conceptual model of three types of subcontinental lithospheric mantle. The model of relationships beneath Central Sudetes is based on findings of Mazur et al. (2015). The hatched red box shows the mantle profiles described and/or interpreted in this study.

Declaration of interests

The authors declare that they have no known competing financial interests or personal relationships that could have appeared to influence the work reported in this paper.

Table 1. Summary of petrographic and mineral chemical data of Dreihausen (Vogelsberg) xenoliths.

Sample	Longest	Modal composition				Rock	% Fo	Mg# opx	Al opx [a	Mg# cpx	Al cpx [a	Cr#
380	11	5	2	13	4	lherzolite	8	0.	0.	0.	0.	0
380	10	5	2	15	3	lherzolite	9	0.	0.	0.	0.	0
380	8	6	2	11	1	lherzolite	9	0.	0.	0.	0.	0
381	7	5	3	1.	4	harzburgite	9	0.	0.	0.	0.	0
381 4	8	2 0.0	7 6.7	3. 3	(	olivine orthopyroxenite	8 7.2-87.6	0. 885	0. 14	0. 870	0. 23	-
381	5	7	2	tra	1	harzburgite	9	0.	0.	-	-	0
381	8	5	3	11	1	lherzolite	8	0.	0.	0.	0.	0
382	5	6	2	6.	4	lherzolite	8	0.	0.	0.	0.	0
382	5	6	2	9.	1	lherzolite	8	0.	0.	0.	0.	0
382	5	6	2	6.	3	lherzolite	9	0.	0.	0.	0.	0
383	5	7	2	2.	(	lherzolite	9	0.	0.	-	-	0
383	4	5	3	8.	3	lherzolite	8	0.	0.	0.	0.	-
384	5	6	2	7.	2	lherzolite	8	0.	0.	0.	0.	0
384	4	7	2	6.	1	lherzolite	9	0.	0.	0.	0.	0

Table 2. Summary of petrographic and mineral chemical data of Allègre and Alleyras (Massif Central) xenoliths.

Sample	Longest	Modal composition				Rock	% Fo	Mg# opx	Al opx [a	Mg# cpx	Al cpx [a	Cr # spl
378	7	5	3	8	4	lherzolit	9	0.	0.	0.	0.	0.
378	4*	5	3	6	5	lherzolit	8	0.	0.	0.	0.	0.
378	7*	5	2	1	2	lherzolit	8	0.	0.	0.	0.	0.
379	6*	7	1	6	0	lherzolit	8	0.	0.	0.	0.	0.
379	4*	8	1	2	0	harzbur	9	0.	0.	0.	0.	0.
379	3*	6	2	1	5	lherzolit	8	0.	0.	0.	0.	0.
379	5*	5	2	1	2	lherzolit	8	0.	0.	0.	0.	0.
379	4*	7	2	5	1	lherzolit	8	0.	0.	0.	0.	0.
374	9	5	2	1	0	lherzolit	8	0.	0.	0.	0.	0.
374	5	4	3	1	4	lherzolit	8	0.	0.	0.	0.	0.
376	5	7	1	1	1	lherzolit	9	0.	0.	0.	0.	0.
376	5	8	1	1	0	harzbu	9	0.	0.	0.	0.	0.
376	6	6	1	1	1	lherzolit	8	0.	0.	0.	0.	0.
376	4	5	3	7	5	lherzolit	8	0.	0.	0.	0.	0.

* - xenolith without any host rock, probably of original size greater than that given in the table.

Highlights

- Mantle root of Variscan Orogen in Europe consists of domains of different nature
- Depleted harzburgites underlie terrane margins (Lower Silesia, north Massif Central)
- Mantle beneath Vogelsberg (Rhine Rift) was strongly modified during Cenozoic rifting
- Refertilised lherzolitic mantle occurs beneath southern Massif Central

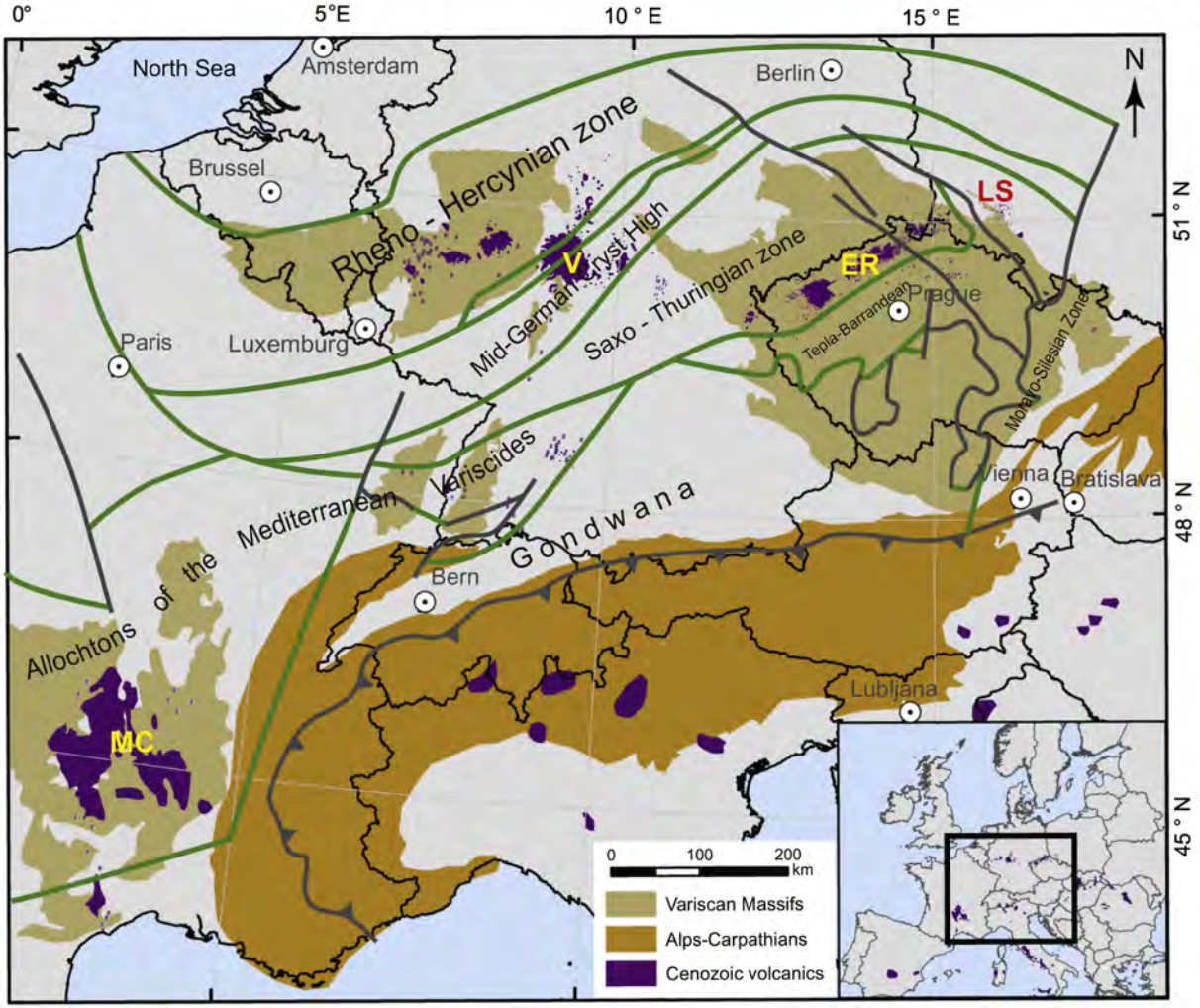
0°
5°E
10 ° E
15 ° E
N
51 ° N
48 ° N
45 ° N
North Sea
Amsterdam
Berlin
Brussel
Rheno - Hercynian zone
V
Mid-German Cryst.High
Saxo - Thuringian zone
LS
ER
Prague
Tepla-Barrandean
Moldanubian Zone
Paris
Luxemburg
Vienna
Bratislava
Variscides
Mediterranean
Gondwana
Bern
Allochtons of the
MC
Ljubljana
0
100
200
km
Variscan Massifs
Alps-Carpathians
Cenozoic volcanics

Figure 1

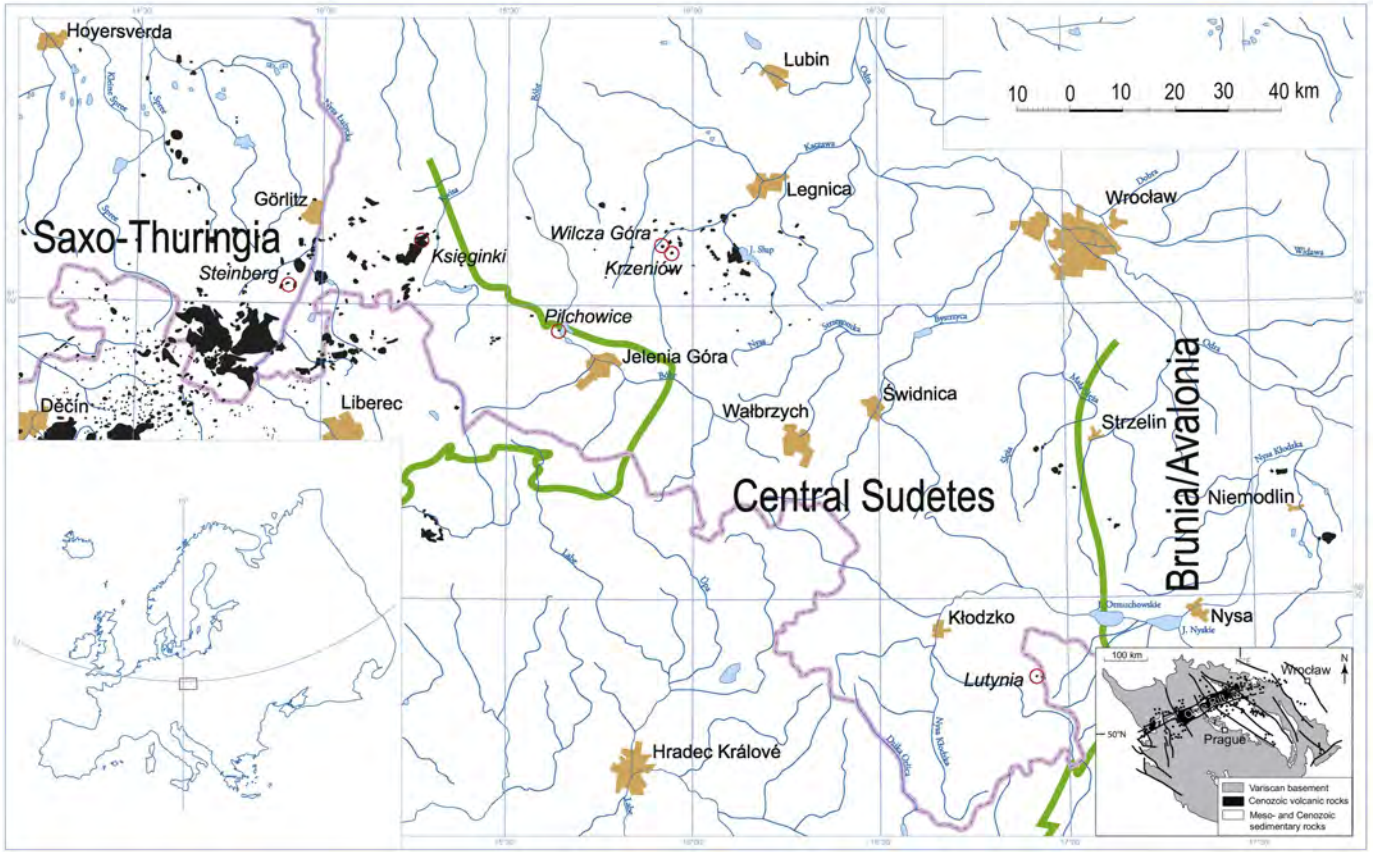
Hoyerswerda
Görlitz
Saxo-Thuringia
Steinberg
Děčín
Liberec
Księginki
Pilchowice
Wilcza Góra
Krzeniów
Lubin
Legnica
Jelenia Góra
Wałbrzych
Świdnica
Wrocław
Strzelin
Brunia/Avalonia
Niemodlin
Central Sudetes
Kłodzko
Nysa
Lutynia
Hradec Králové
10 0 10 20 30 40 km
100 km
50°N
Prague
Variscan basement
Cenozoic volcanic rocks
Meso- and Cenozoic sedimentary rocks

Figure 2

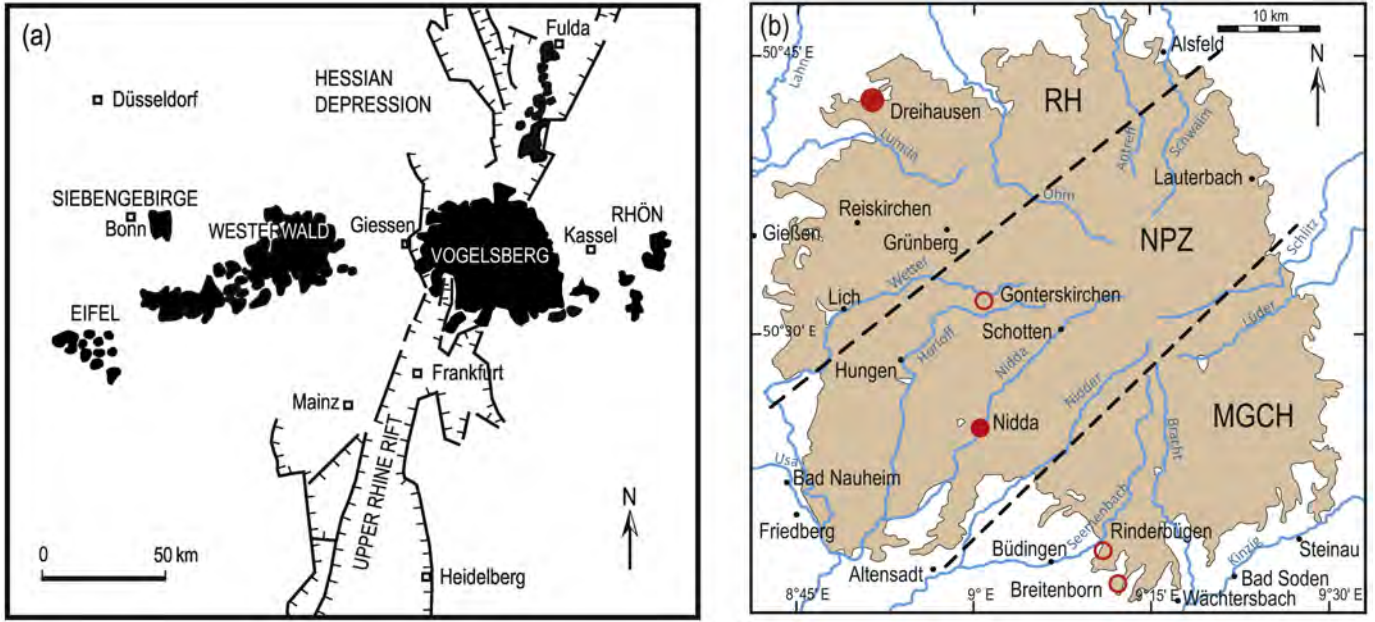
(a)
Düsseldorf
HESSIAN
DEPRESSION
Fulda
SIEBENGEBIRGE
Bonn
WESTERWALD
Giessen
VOGELSBERG
Kassel
RHÖN
EIFEL
Frankfurt
Mainz
UPPER RHINE RIFT
Heidelberg
0
50 km
N
(b)
10 km
50°45' E
Alsfeld
N
Lahn
Dreihausen
RH
Lumda
Ohm
Antreff
Schwalm
Lauterbach
Reiskirchen
Gießen
Grünberg
NPZ
Schlitz
Wetter
Lich
Gonterskirchen
50°30' E
Schotten
Lüder
Hungen
Horloff
Nidda
Hiddar
Nidda
MGCH
Braht
Usa
Bad Nauheim
Friedberg
Seemenbach
Rinderbügen
Büdingen
Steinau
Kinzig
Altensadt
8°45' E
9° E
Breitenborn
9°15' E
Wächtersbach
Bad Soden
9°30' E

Figure 3

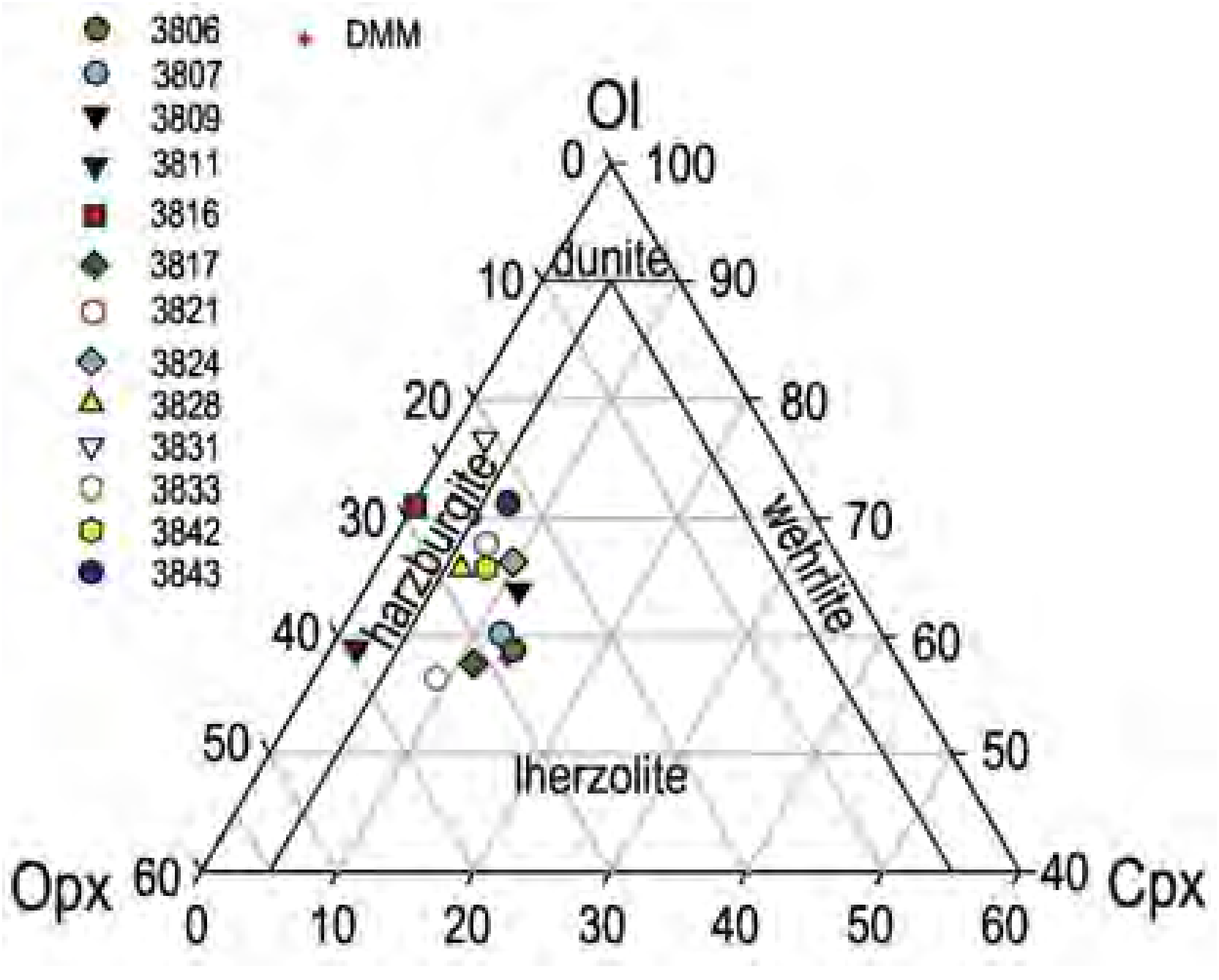
3806
3807
3809
3811
3816
3817
3821
3824
3828
3831
3833
3842
3843
DMM
Ol
0
100
10
dunite
90
20
80
30
harzburgite
wehrlite
70
40
60
50
lherzolite
50
Opx
60
0
10
20
30
40
50
60
40
Cpx

Figure 4

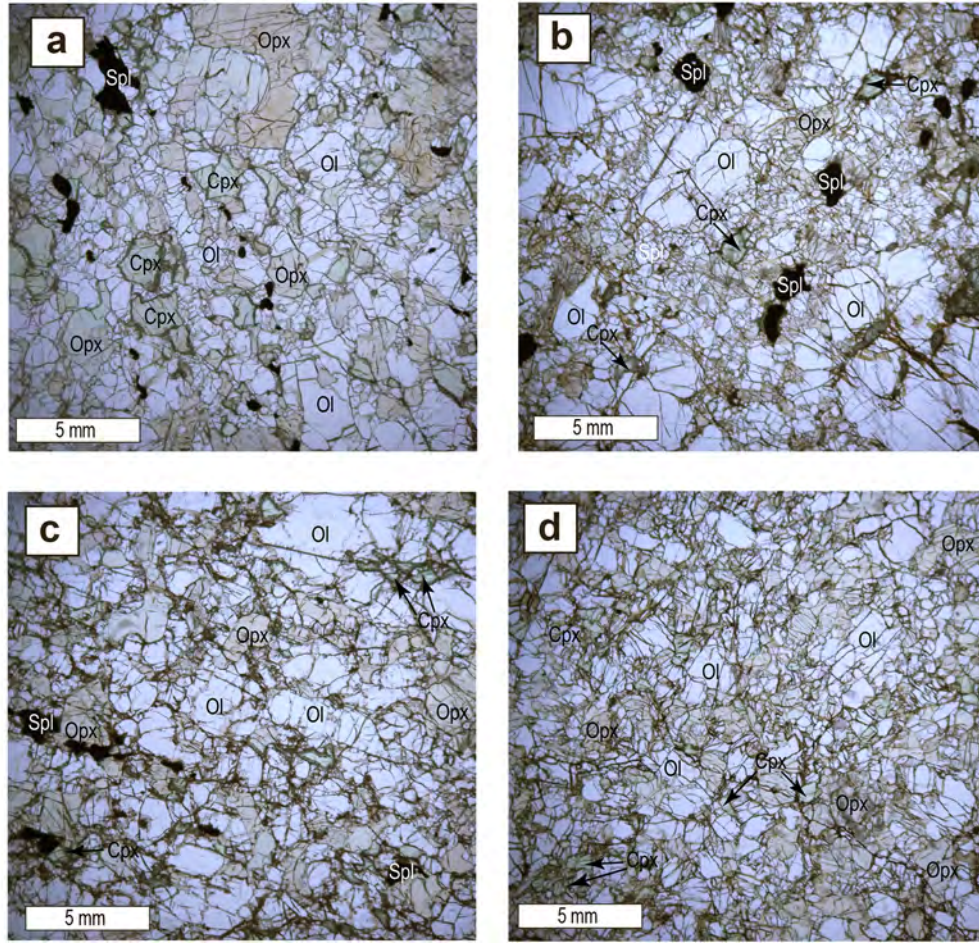
a
Opx
Spl
Ol
Cpx
Cpx
Ol
Opx
Cpx
Opx
Ol
5 mm
b
Spl
Cpx
Opx
Ol
Spl
Cpx
Spl
Spl
Ol
Ol
Cpx
5 mm
c
Ol
Cpx
Opx
Ol
Ol
Opx
Spl
Opx
Cpx
Spl
5 mm
d
Opx
Cpx
Ol
Ol
Opx
Ol
Cpx
Opx
Cpx
Opx
5 mm

Figure 5

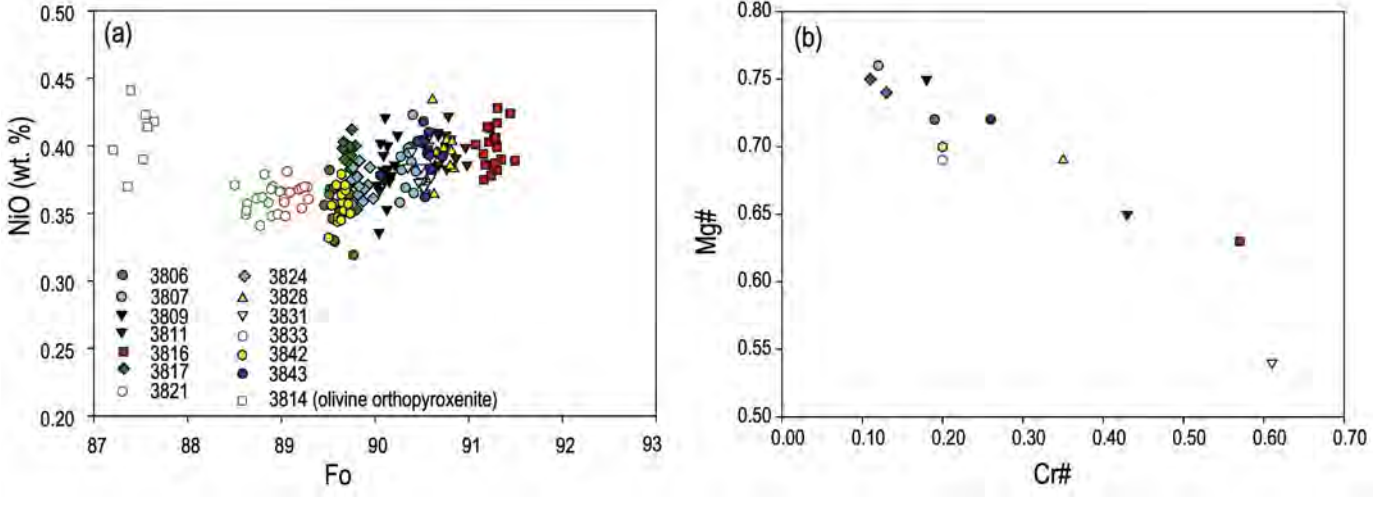
(a)
NiO (wt. %)
Fo
3806
3807
3809
3811
3816
3817
3821
3824
3828
3831
3833
3842
3843
3814 (olivine orthopyroxenite)
(b)
Mg#
Cr#

Figure 6

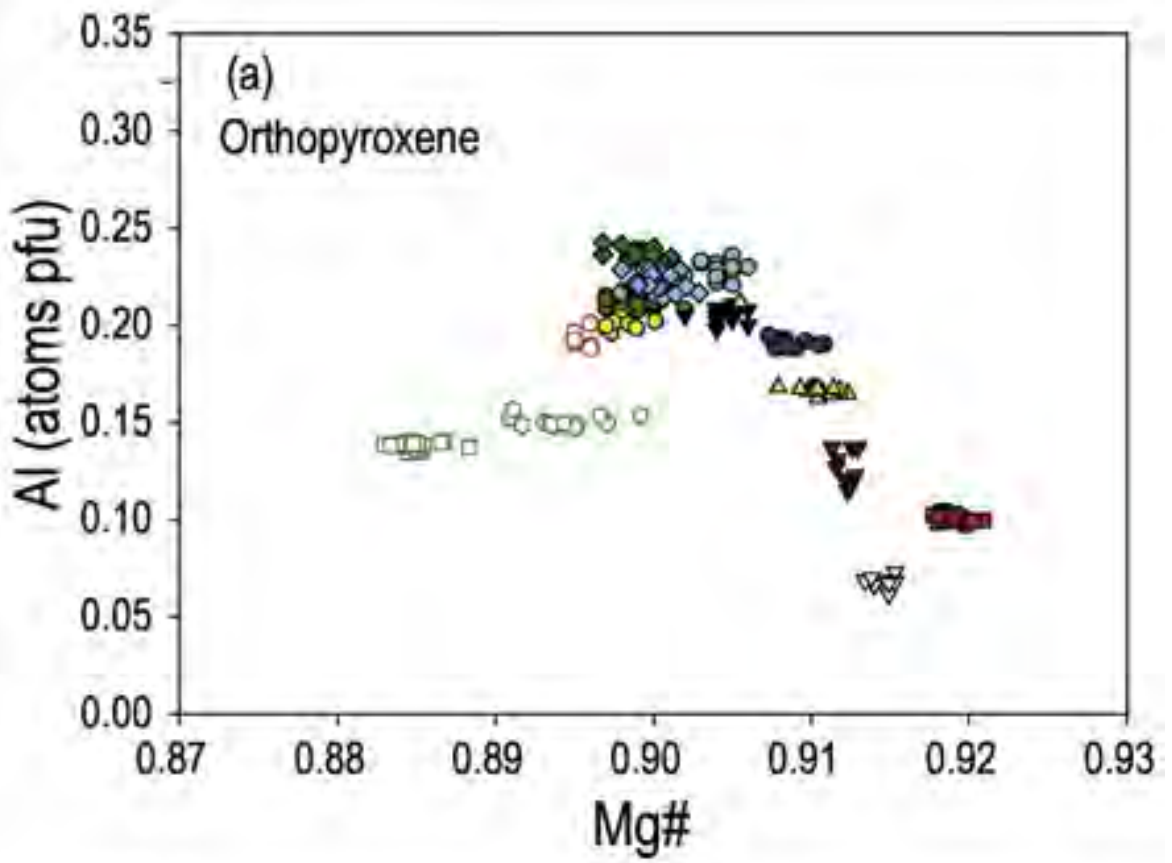
(a)
Orthopyroxene
Al (atoms pfu)
0.35
0.30
0.25
0.20
0.15
0.10
0.05
0.00
0.87
0.88
0.89
0.90
0.91
0.92
0.93
Mg#

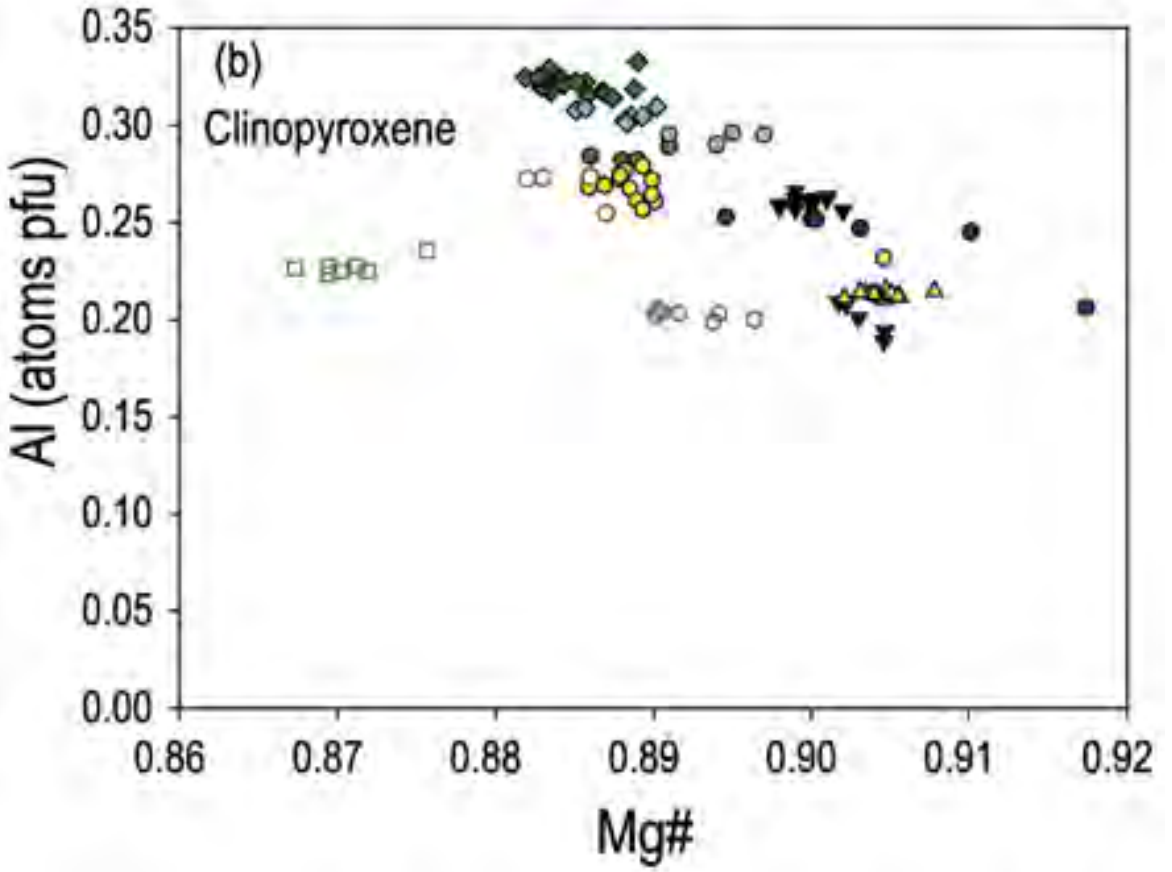
(b)
Clinopyroxene
Al (atoms pfu)
0.35
0.30
0.25
0.20
0.15
0.10
0.05
0.00
0.86
0.87
0.88
0.89
0.90
0.91
0.92
Mg#

Figure 7

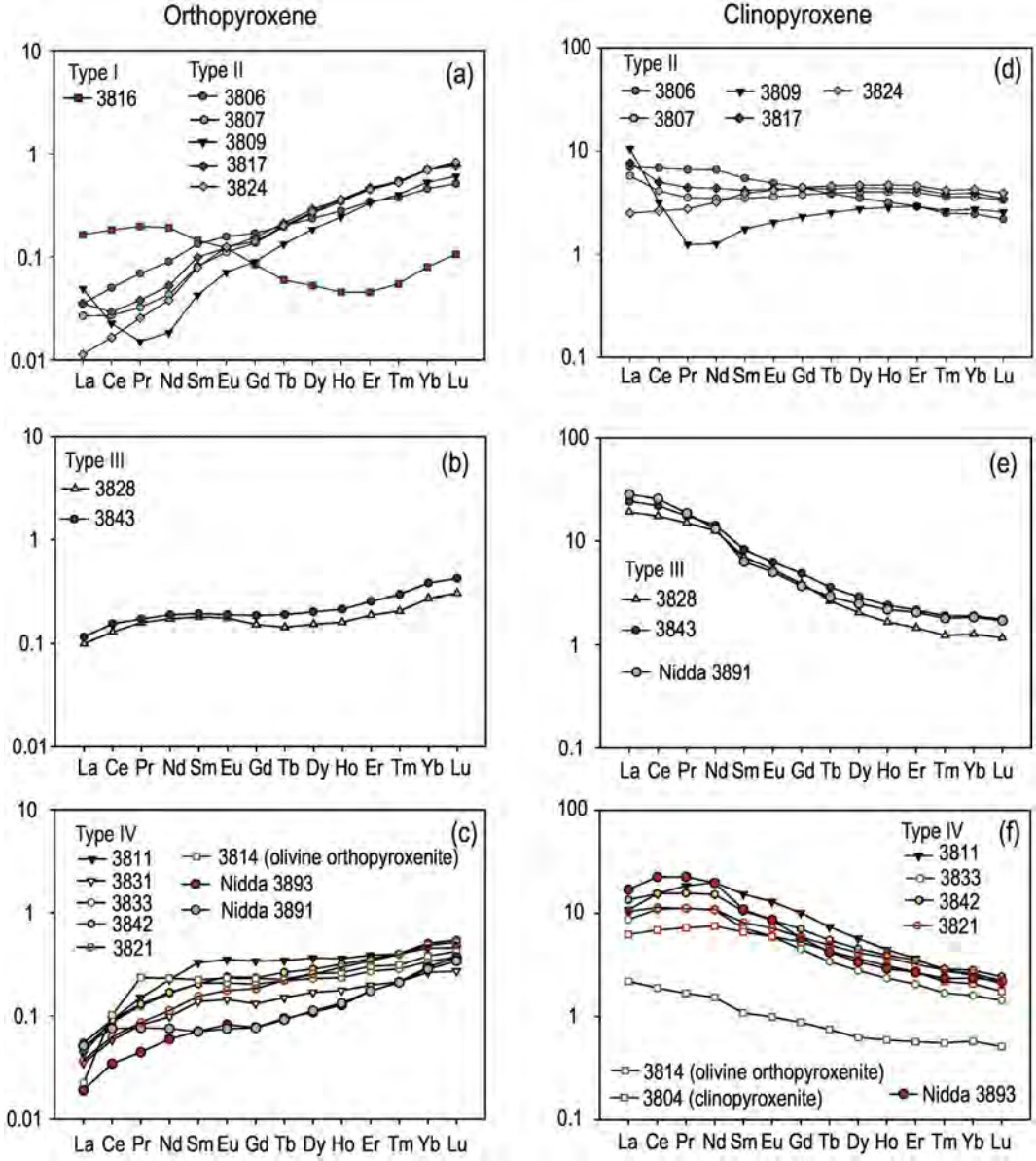
Orthopyroxene
Clinopyroxene
Type I
3816
Type II
3806
3807
3809
3817
3824
(a)
Type II
3806
3809
3824
3807
3817
(d)
Type III
3828
3843
(b)
3828
3843
Nidda 3891
(e)
Type IV
3811
3831
3833
3842
3821
3814 (olivine orthopyroxenite)
Nidda 3893
Nidda 3891
(c)
Type IV
3811
3833
3842
3821
(f)
3814 (olivine orthopyroxenite)
3804 (clinopyroxenite)
Nidda 3893
La Ce Pr Nd Sm Eu Gd Tb Dy Ho Er Tm Yb Lu

Figure 8

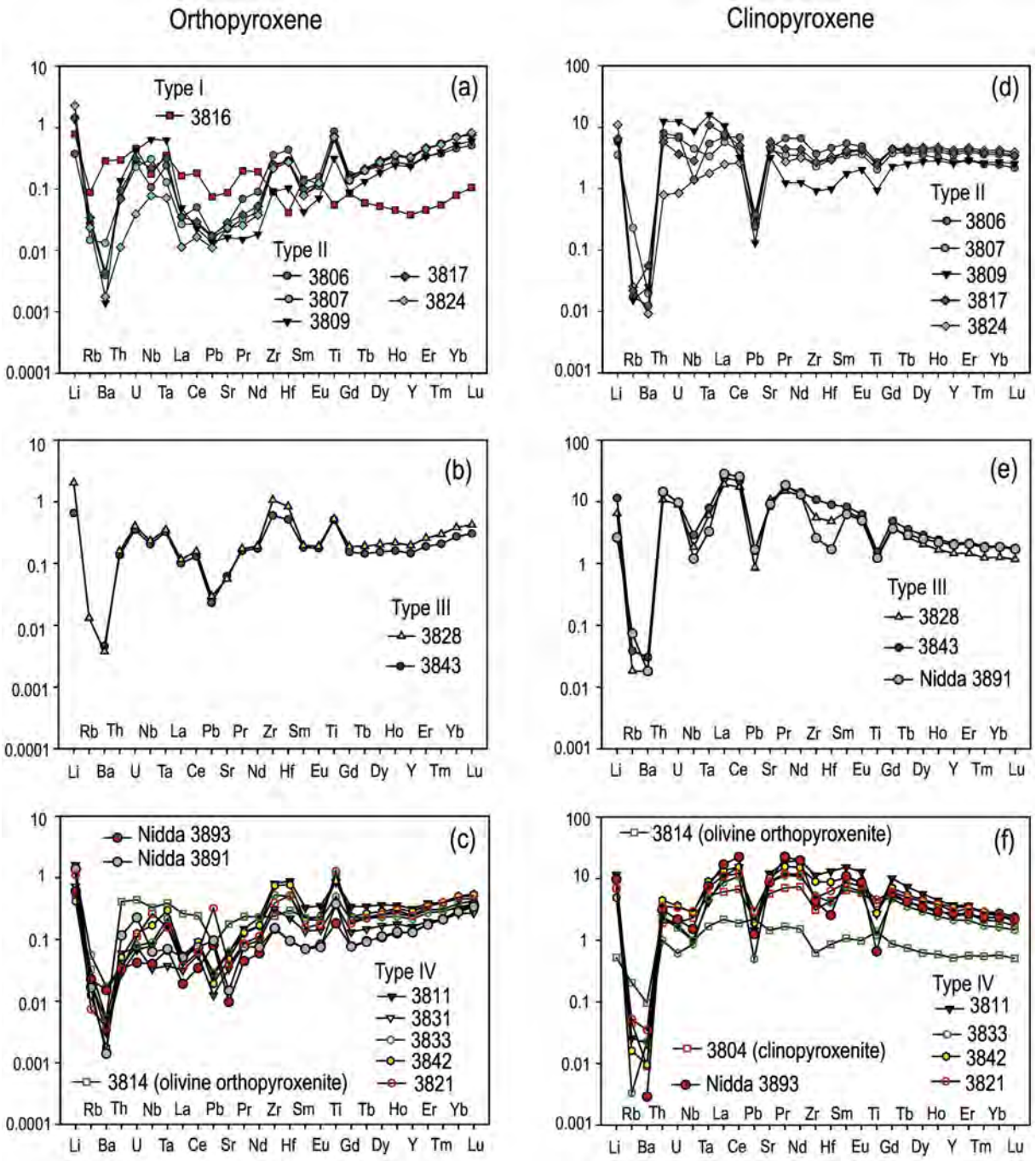
Orthopyroxene
Clinopyroxene
(a)
Type I
3816
Type II
3806
3807
3809
3817
3824
(b)
Type III
3828
3843
(c)
Nidda 3893
Nidda 3891
Type IV
3811
3831
3833
3842
3821
3814 (olivine orthopyroxenite)
(d)
Type II
3806
3807
3809
3817
3824
(e)
Type III
3828
3843
Nidda 3891
(f)
3814 (olivine orthopyroxenite)
Type IV
3811
3833
3842
3821
3804 (clinopyroxenite)
Nidda 3893
Rb Th Nb La Pb Pr Zr Sm Ti Tb Ho Er Yb
Li Ba U Ta Ce Sr Nd Hf Eu Gd Dy Y Tm Lu

Figure 9

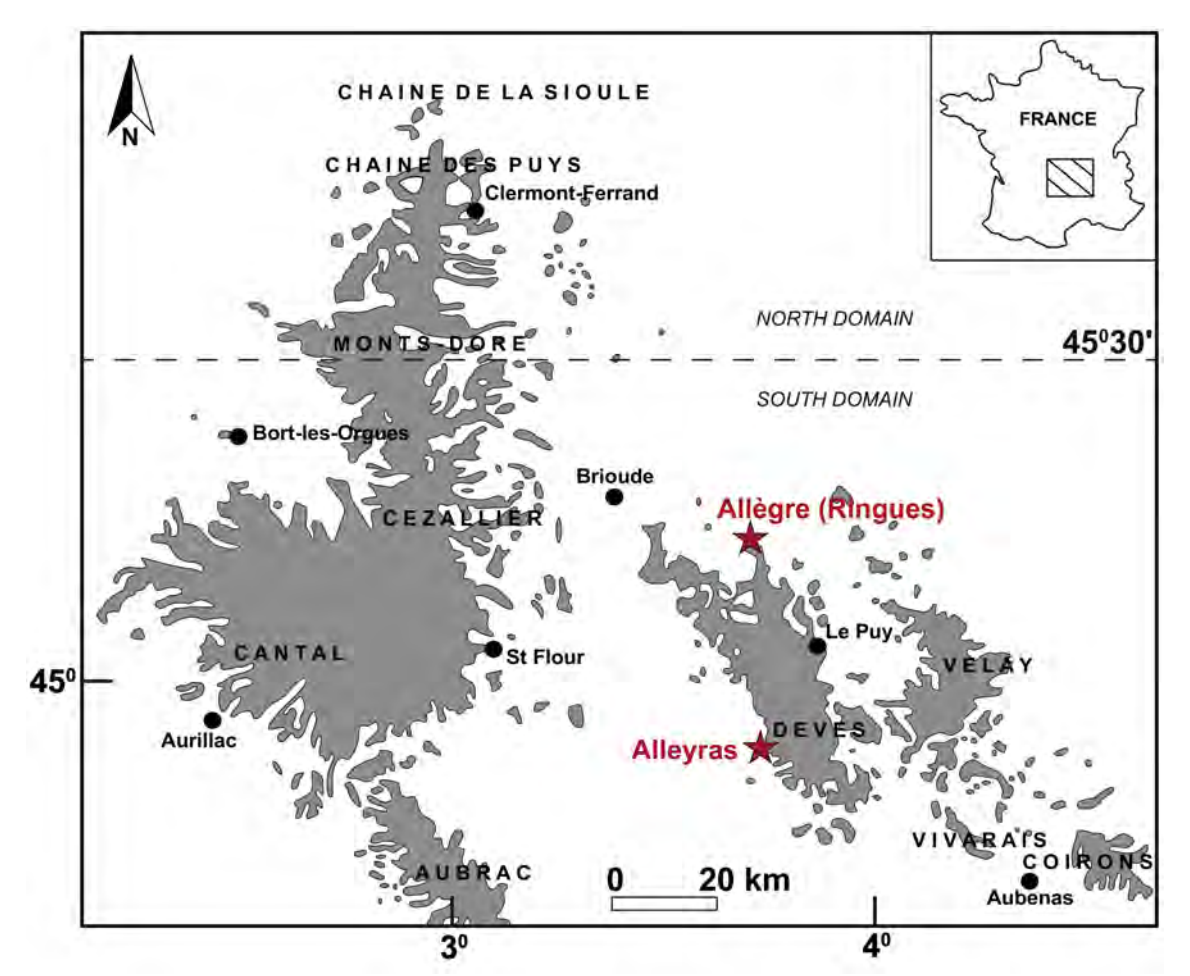
N
CHAINE DE LA SIOULE
CHAINE DES PUYS
Clermont-Ferrand
FRANCE
NORTH DOMAIN
MONTS-DORE
45°30'
SOUTH DOMAIN
Bort-les-Orgues
Brioude
Allègre (Ringues)
CEZALLIER
Le Puy
CANTAL
St Flour
VELAY
45°
Aurillac
DEVES
Alleyras
VIVARAIS
COIRONS
AUBRAC
0
20 km
Aubenas
3°
4°

Figure 10

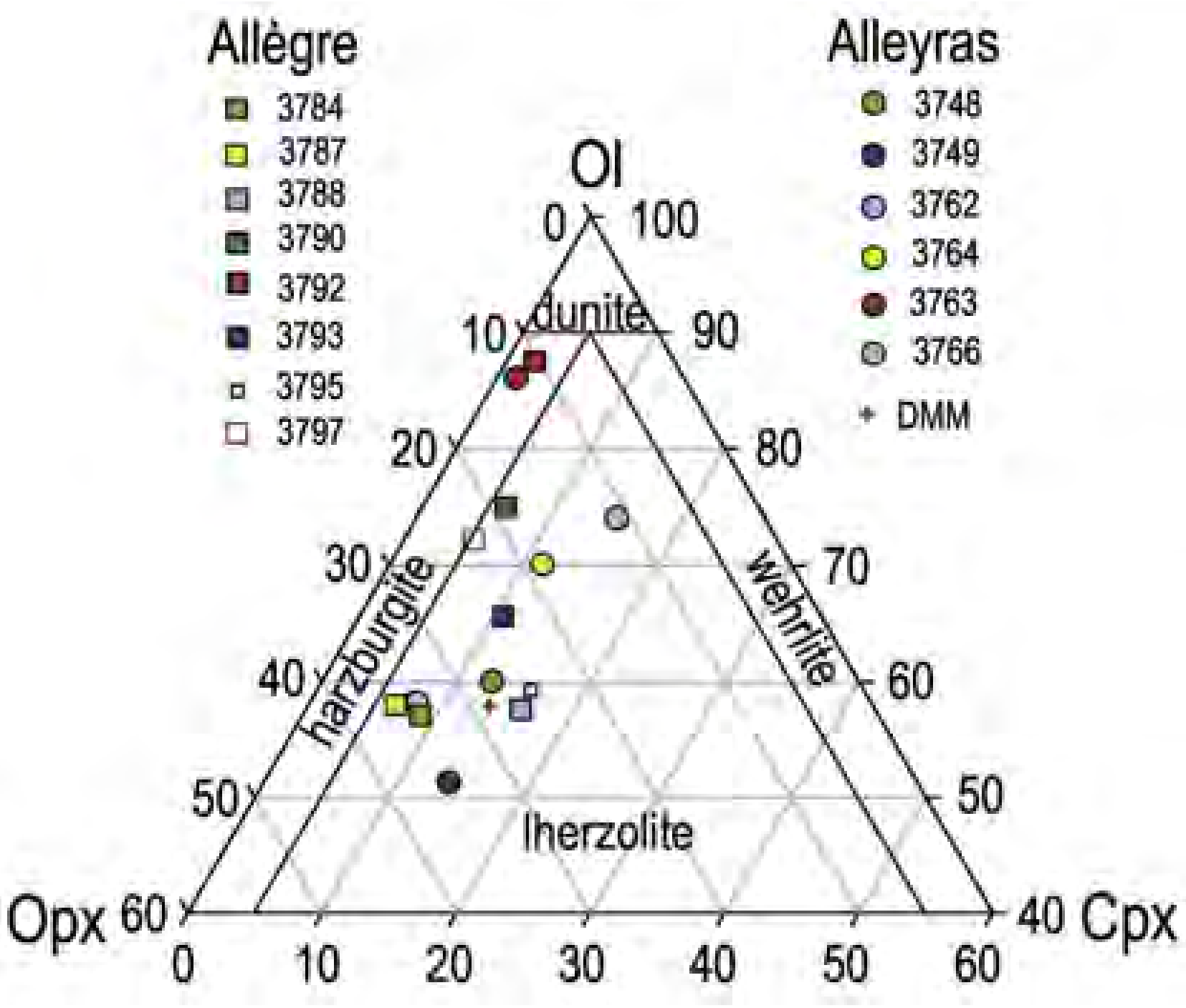
Allègre
3784
3787
3788
3790
3792
3793
3795
3797
Alleyras
3748
3749
3762
3764
3763
3766
DMM
Ol
0
100
10
90
20
80
30
70
40
60
50
50
60
40
dunite
harzburgite
wehrlite
lherzolite
Opx
Cpx
0
10
20
30
40
50
60

Figure 11

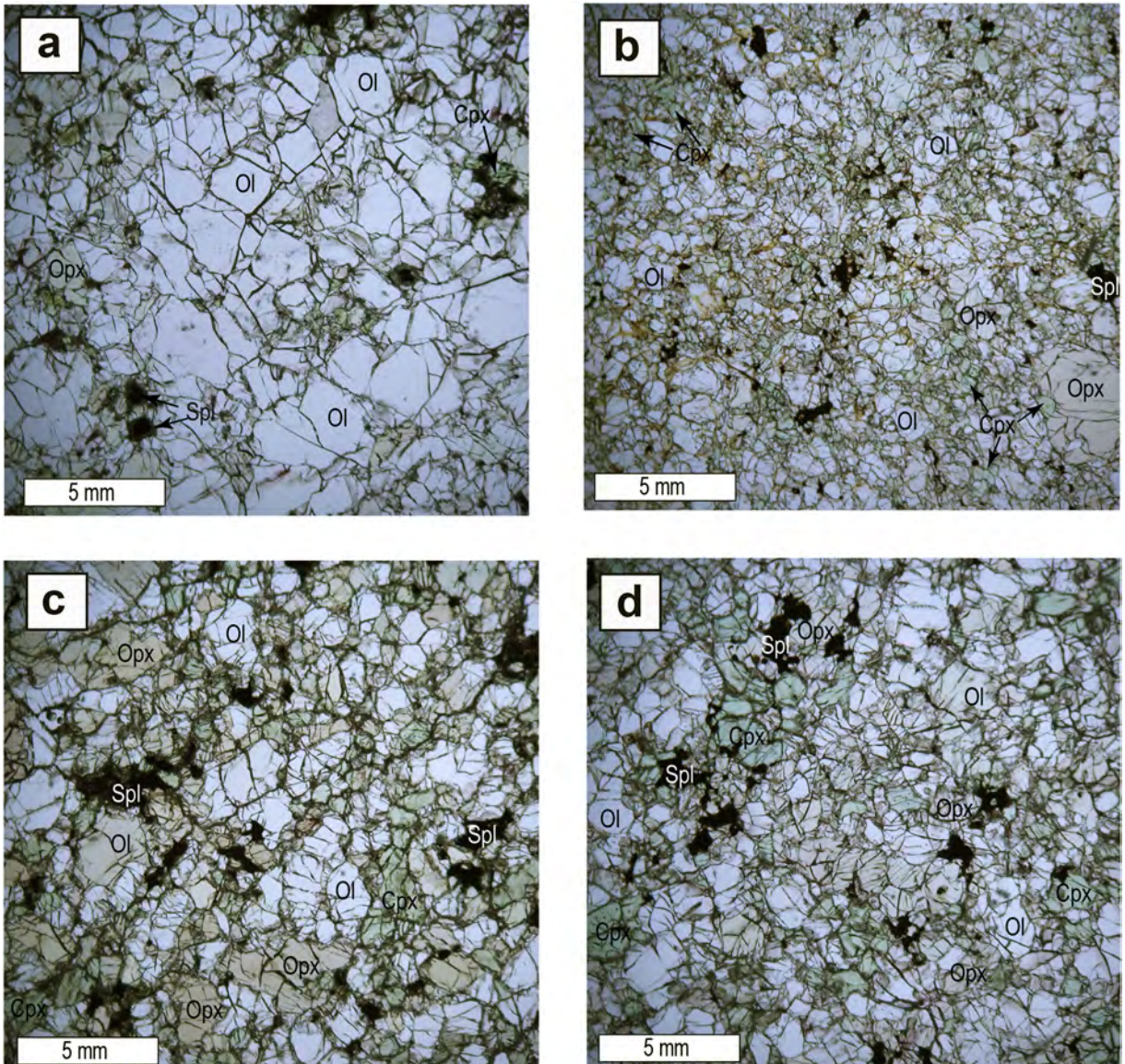
a
Ol
Cpx
Ol
Opx
Spl
Ol
5 mm
b
Cpx
Ol
Ol
Spl
Opx
Opx
Ol
Cpx
5 mm
c
Opx
Ol
Spl
Spl
Ol
Ol
Cpx
Opx
Cpx
Opx
5 mm
d
Spl
Opx
Ol
Cpx
Spl
Ol
Opx
Cpx
Cpx
Ol
Opx
5 mm

Figure 12

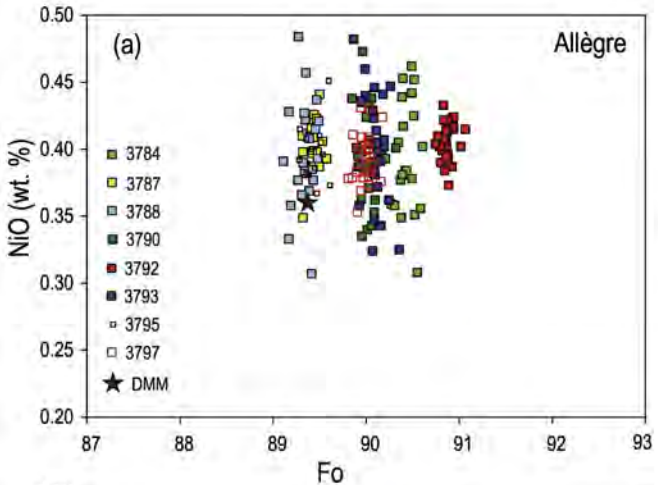
(a)
Allègre
NiO (wt. %)
Fo
3784
3787
3788
3790
3792
3793
3795
3797
DMM

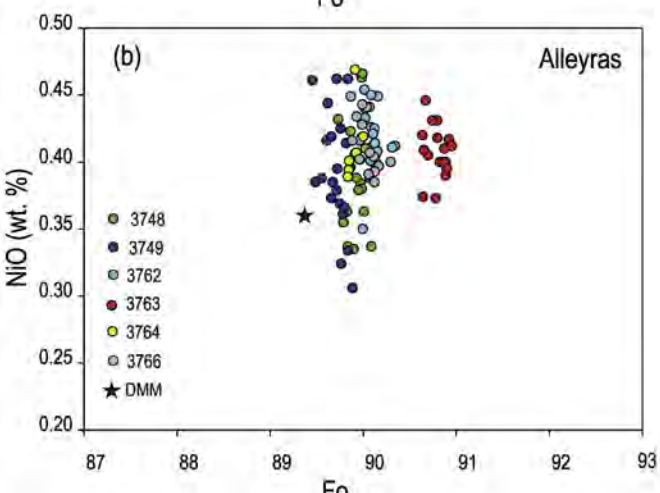
(b)
Alleyras
NiO (wt. %)
Fo
3748
3749
3762
3763
3764
3766
DMM

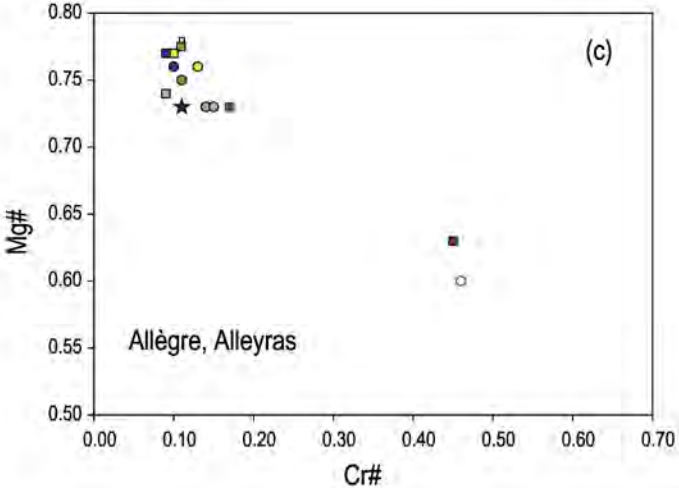
(c)
Mg#
Cr#
Allègre, Alleyras

Figure 13

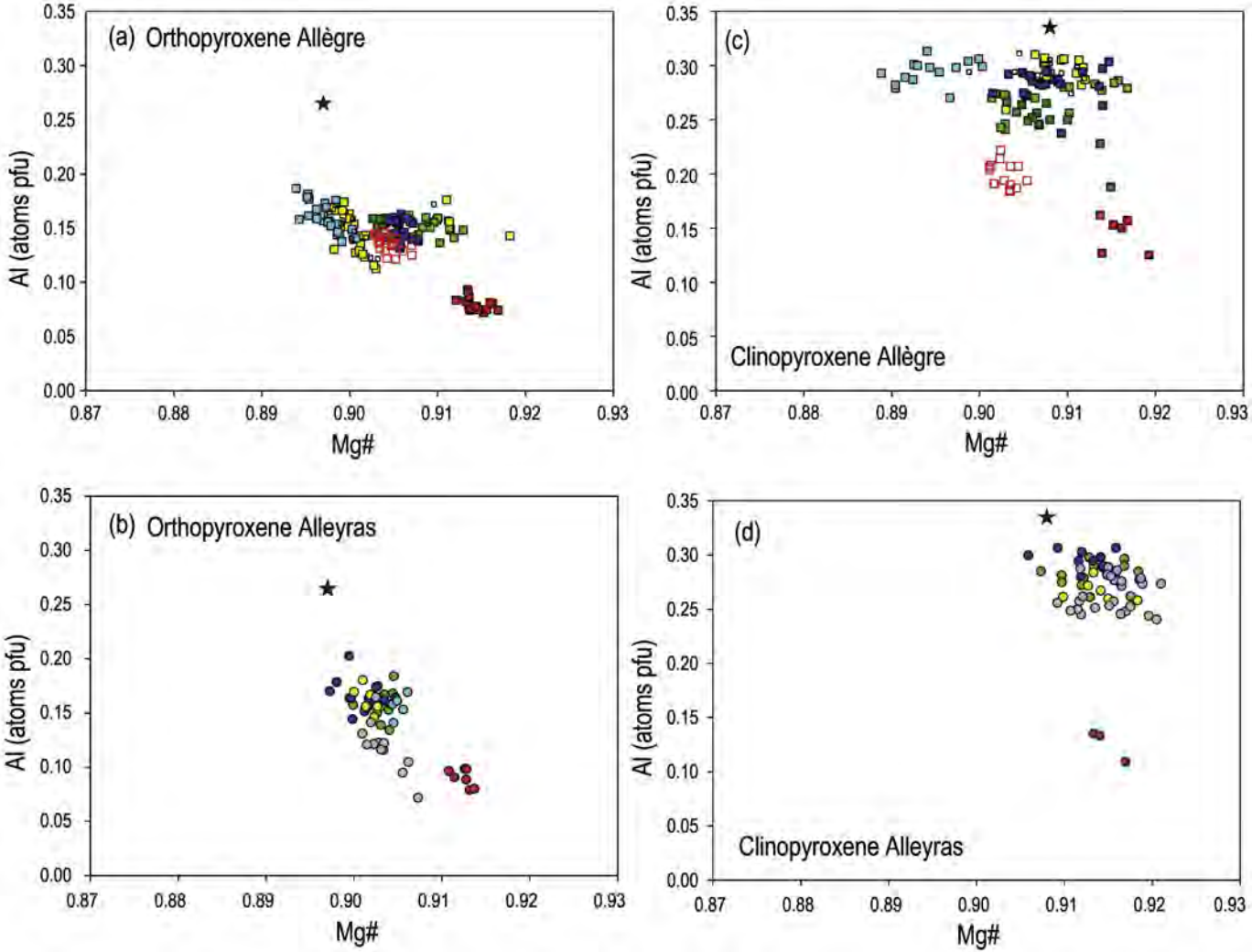
(a) Orthopyroxene Allègre
(c)
Clinopyroxene Allègre
(b) Orthopyroxene Alleyras
(d)
Clinopyroxene Alleyras
Al (atoms pfu)
Mg#
0.35
0.30
0.25
0.20
0.15
0.10
0.05
0.00
0.87
0.88
0.89
0.90
0.91
0.92
0.93

Figure 14

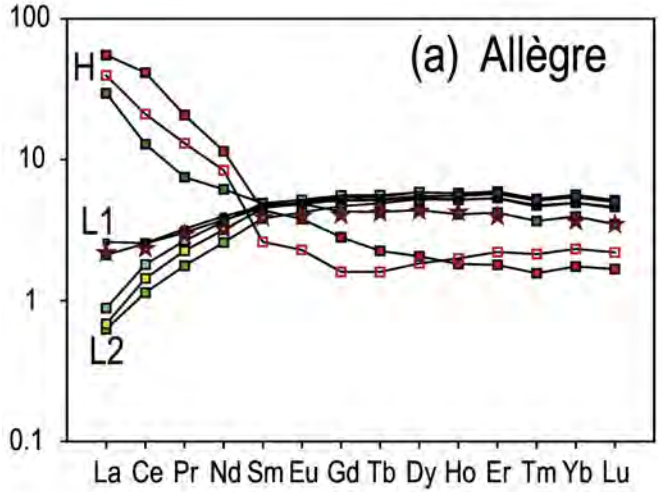
(a) Allègre
H
L1
L2
100
10
1
0.1
La Ce Pr Nd Sm Eu Gd Tb Dy Ho Er Tm Yb Lu

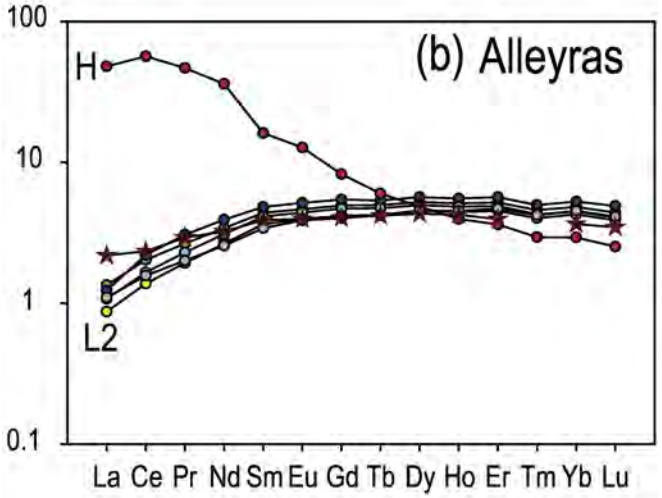
(b) Alleyras
H
L2
100
10
1
0.1
La Ce Pr Nd Sm Eu Gd Tb Dy Ho Er Tm Yb Lu

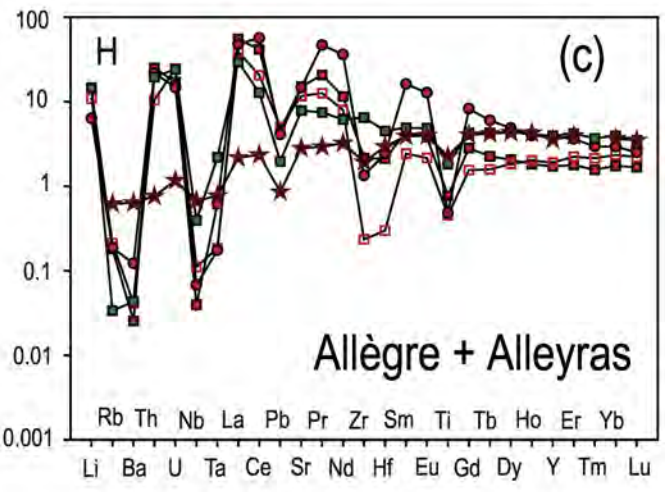
(c)
H
Allègre + Alleyras
100
10
1
0.1
0.01
0.001
Rb Th Nb La Pb Pr Zr Sm Ti Tb Ho Er Yb
Li Ba U Ta Ce Sr Nd Hf Eu Gd Dy Y Tm Lu

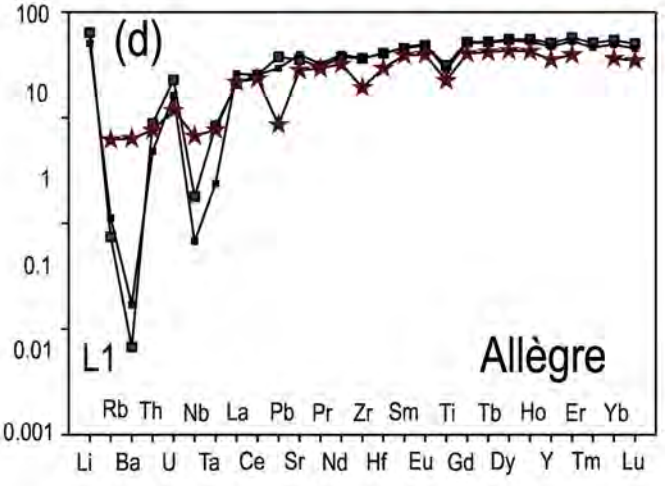
(d)
L1
Allègre
100
10
1
0.1
0.01
0.001
Rb Th Nb La Pb Pr Zr Sm Ti Tb Ho Er Yb
Li Ba U Ta Ce Sr Nd Hf Eu Gd Dy Y Tm Lu

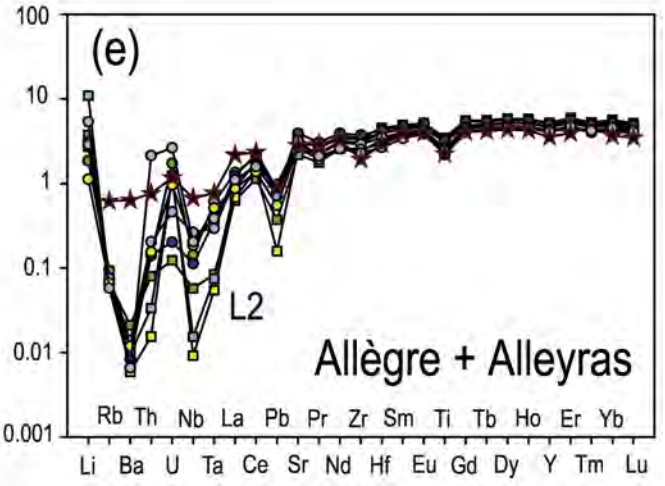
(e)
L2
Allègre + Alleyras
100
10
1
0.1
0.01
0.001
Rb Th Nb La Pb Pr Zr Sm Ti Tb Ho Er Yb
Li Ba U Ta Ce Sr Nd Hf Eu Gd Dy Y Tm Lu

Figure 15

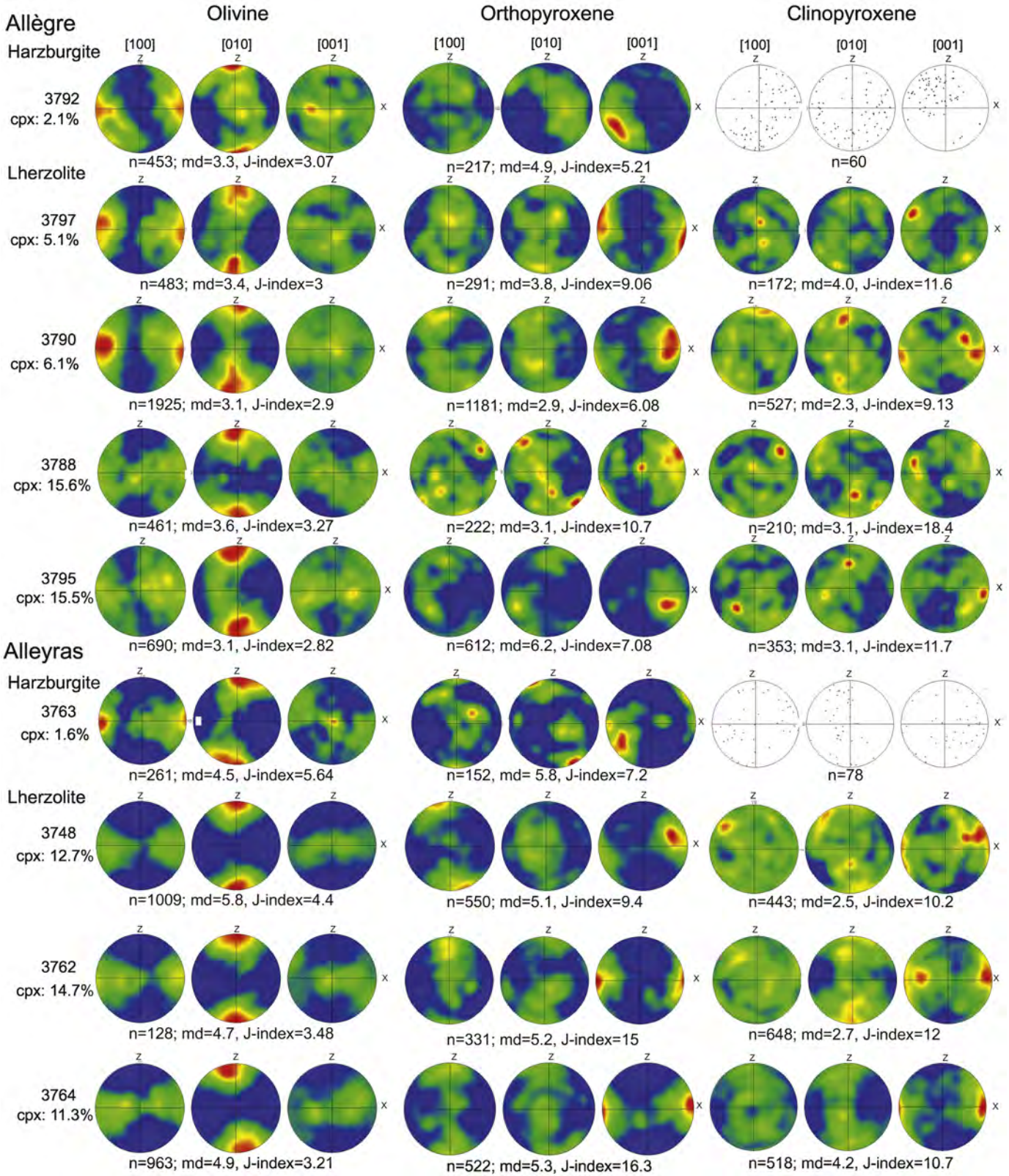
Allègre
Olivine
Orthopyroxene
Clinopyroxene
[100]
[010]
[001]
Harzburgite
3792
cpx: 2.1%
n=453; md=3.3, J-index=3.07
n=217; md=4.9, J-index=5.21
n=60
Lherzolite
3797
cpx: 5.1%
n=483; md=3.4, J-index=3
n=291; md=3.8, J-index=9.06
n=172; md=4.0, J-index=11.6
3790
cpx: 6.1%
n=1925; md=3.1, J-index=2.9
n=1181; md=2.9, J-index=6.08
n=527; md=2.3, J-index=9.13
3788
cpx: 15.6%
n=461; md=3.6, J-index=3.27
n=222; md=3.1, J-index=10.7
n=210; md=3.1, J-index=18.4
3795
cpx: 15.5%
n=690; md=3.1, J-index=2.82
n=612; md=6.2, J-index=7.08
n=353; md=3.1, J-index=11.7
Alleyras
Harzburgite
3763
cpx: 1.6%
n=261; md=4.5, J-index=5.64
n=152, md= 5.8, J-index=7.2
n=78
Lherzolite
3748
cpx: 12.7%
n=1009; md=5.8, J-index=4.4
n=550; md=5.1, J-index=9.4
n=443; md=2.5, J-index=10.2
3762
cpx: 14.7%
n=128; md=4.7, J-index=3.48
n=331; md=5.2, J-index=15
n=648; md=2.7, J-index=12
3764
cpx: 11.3%
n=963; md=4.9, J-index=3.21
n=522; md=5.3, J-index=16.3
n=518; md=4.2, J-index=10.7

Figure 16

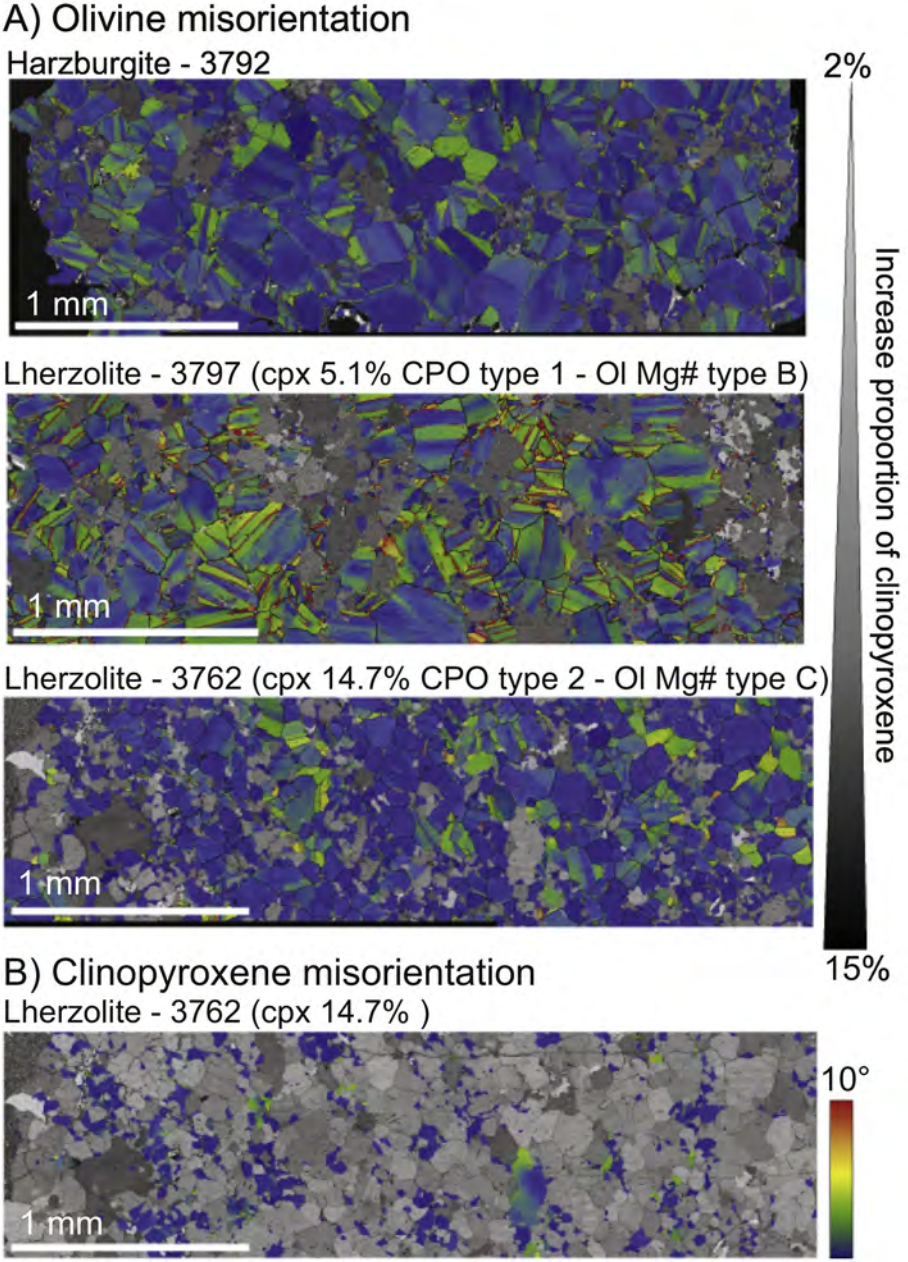
A) Olivine misorientation
Harzburgite - 3792
1 mm
Lherzolite - 3797 (cpx 5.1% CPO type 1 - Ol Mg# type B)
1 mm
Lherzolite - 3762 (cpx 14.7% CPO type 2 - Ol Mg# type C)
1 mm
2%
Increase proportion of clinopyroxene
15%
B) Clinopyroxene misorientation
Lherzolite - 3762 (cpx 14.7%)
1 mm
10°

Figure 17

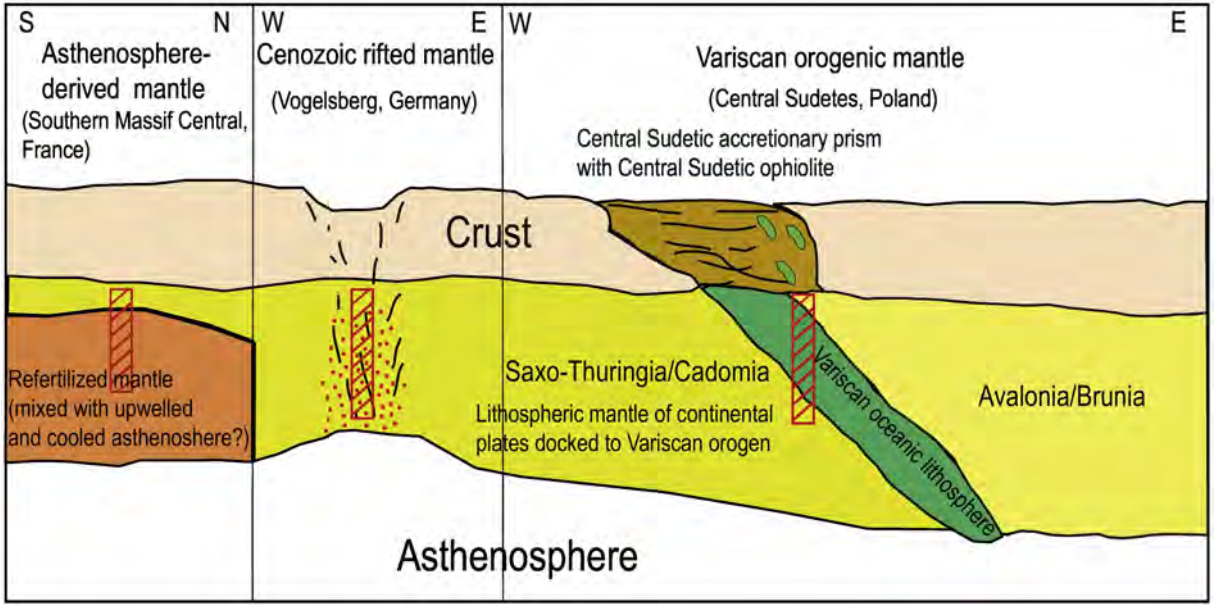
S
N
Asthenosphere-derived mantle
(Southern Massif Central, France)
W
E
Cenozoic rifted mantle
(Vogelsberg, Germany)
W
E
Variscan orogenic mantle
(Central Sudetes, Poland)
Central Sudetic accretionary prism with Central Sudetic ophiolite
Crust
Refertilized mantle (mixed with upwelled and cooled asthenoshere?)
Saxo-Thuringia/Cadomia
Lithospheric mantle of continental plates docked to Variscan orogen
Variscan oceanic lithosphere
Avalonia/Brunia
Asthenosphere

Figure 18